*Physics – Uspekhi* **54** (12) 1203 – 1225 (2011) 

*REVIEWS OF TOPICAL PROBLEMS* PACS numbers: 41.20.Cv, **67.25.–k**, 68.03.Hj

# Instability and reconstruction of a charged liquid surface

V B Shikin

DOI: 10.3367/UFNe.0181.201112a.1241

## Contents



**Abstract. This review presents a systematic summary of the information collected to date on the instability and reconstruction of the flat charged surface of a cryogenic liquid under various conditions in terms of unit cell geometry, external electrostatics, filling degree, etc. Prospects for future research are explored.**

## 1. Introduction

The problem of the instability of a charged liquid surface arose in the 1930s in connection with the discovery of the decay of heavy atomic nuclei. Frenkel [1, 2] and, independently, Bohr and Wheeler [3] were the first to offer an acceptable explanation of this fundamental phenomenon based on the liquid-drop model. An earlier and less-known variant of the problem concerning the oscillation spectrum of a flat charged liquid surface (Frenkel [4, 5] and Tonks [6]) attracted in essence significant attention only in the 1970s, when extensive studies of the properties of various low-dimensional charged structures began. One of them, a two-dimensional (2D) charged system at the surface of liquid dielectrics (helium, hydrogen, etc.), is to a large extent controlled by the Frenkel–Tonks (FT) effect [4–6], since the instability predicted by these authors places an upper bound on charged particle density at the surface of a liquid dielectric. By that time, research in this field had extended to encompass natural generalization of the FT theory for interfaces between two liquid dielectrics [7, 8] or magnetic substances [9]. In the latter case, the point in question is simulation of a liquid magnet with a suspension of solid magnetic particles.

A characteristic feature of FT phenomenon distinguishing it from other known decays (Rayleigh instability of a cylindrical jet [10], Karman trace behind a moving cylinder (sphere) [11], Taylor vortex instability of a viscous liquid layer between two rotating coaxial cylinders [12], instability of the interface between two liquid media moving relative to each other [12], Rayleigh–Benard instability [13], etc.) is the possibility of stopping the decay and forming a new metastable state with a finite corrugation amplitude (i.e., reconstruction of the charged liquid surface).

At different times, the phenomenon of liquid surface reconstruction in external fields has attracted the attention of many researchers [14–27], but the general picture is beginning to emerge only now. In this process, only the initial part of the instability decay has a universal nature (in all cases, the frequency squared of the dispersion law for small oscillations crosses zero and becomes negative). As regards the details of the new metastable corrugated state, it lacks a universal development of events. The chronologically first scenario proposed by Zaitsev and Shliomis [14] for the interface between liquid dielectrics (magnetic substances) in an external field may be arbitrarily regarded as homogeneous, implying preservation of homogeneity of the boundary conditions along the bent surface assumed to be laterally infinite. The majority of subsequent publications [17–27] dealing with details of the homogeneous scenario of liquid surface reconstruction aimed to reduce the problem in question to one of Hamiltonian dynamics, take account of the specificity of concrete systems, and describe the dynamic properties of the appearing lattices in terms of embraced ideology [14].

Clearly, the reconstruction of a charged helium surface under conditions of total charge conservation at the vapor–liquid interface proceeds in a different way. The equipotentiality of the boundary becomes violated (the charges draw together in isolated dimples) with an increase in the degree of corrugation; it affects both the details of the theory being constructed and the corollaries observed. Specifically, aperiodic reconstruction [28] lacking in homogeneous scenarios becomes possible.

The reconstruction of thin helium films, both neutral and charged ones, also proceeds on a qualitatively different basis than that in Ref. [14]. Here, one more important detail

**V B Shikin** Institute of Solid State Physics, Russian Academy of Sciences, ul. Akademika Osip'yana 2, 142432 Chernogolovka, Moscow region, Russian Federation. E-mail: shikin@issp.ac.ru

Received 8 February 2011, revised 27 May 2011
*Uspekhi Fizicheskikh Nauk* **181** (12) 1241 – 1264 (2011)
DOI: 10.3367/UFNr.0181.201112a.1241
Translated by Yu V Morozov; edited by A Radzig

emerges that permits us to regard the reconstruction problem as an inhomogeneous one because the dispersion law is violated in the first place at arbitrarily small wave numbers rather than at finite ones (as in the problem for a liquid half-space). Therefore, the reconstruction problem makes sense only for systems with restricted lateral dimensions.

In light of the aforesaid, it appears natural to discuss the current state of the inhomogeneous reconstruction problem with reference to its homogeneous counterpart, briefly presented in review [16]. The case at hand is nonlinear phenomena occurring on a charged helium (hydrogen) surface. The presence of charges gives, apart from ideological novelty, the possibility of manipulating a wide range of external impacts. Moreover, exploration of the (helium + charges) system is fairly advanced as regards comprehension of nonlinear effects.

It is worthy of special note that external parameters of the problem include various geometric factors, such as the system's dimensions or the presence of a substrate. Nevertheless, the discussion of such nuances does not involve successfully developing lines of research concerned with stability of explicitly nonplanar structures, such as cylindrical and spherical liquid surfaces [1–3, 10, 29–37], i.e., problems arising in research on charged nucleus stability, liquid atomization, raindrop behavior in thunderstorm fields, the rapidly progressing spectroscopy of isolated charged nanodroplets, etc. Consideration of this wide area of research is beyond the scope of the present paper.

## 2. The charged liquid surface

### 2.1 Problem geometry

In starting to study dynamic phenomena on a charged helium surface, we shall first discuss the physical causes responsible for the formation of such states. Free electrons have a negative affinity for liquid helium. In other words, the energy $V_0$ of electron embedding into liquid helium is positive and, what is important, much higher than characteristic helium temperatures. This means that a free electron with a kinetic energy below $V_0$ driven to the liquid helium surface cannot embed into depths of liquid and must remain in the gaseous phase. On the other hand, an electron in a vacuum near the dielectric boundary is attracted to it under the action of image forces, resulting in the appearance of a one-dimensional potential well in which the electron may localize at sufficiently low temperatures. A distinctive feature of bound electron states over helium is a relatively low binding energy due to the weak polarizability of liquid helium. As a result, electrons are 'suspended' at a macroscopic distance (some $10^{-6}$ cm) above the free helium surface.

An important methodical feature inevitably inherent in experiments with electrons above the helium surface is the presence of a metallic substrate. Being similarly charged particles, electrons cannot co-exist in a uniform state at a finite number density, $n_s \neq 0$. To achieve this desired result, a 2D electron system is positioned over a metal surface to create a structure resembling a plane capacitor with the constant $n_s$ substantially maintained in the lateral direction.

Let us consider the system presented in Fig. 1a. The space between two plates of the plane-parallel capacitor is partly filled with liquid helium; $h$, $h-d$, and $d$ are the distance between the plates, the vacuum gap, and the helium layer thickness in the capacitor, respectively. The $z$-axis is normal

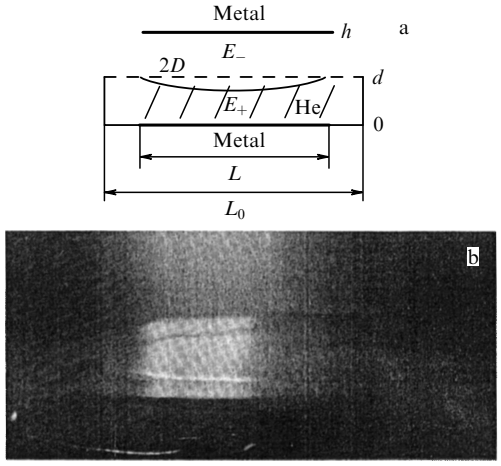


**Figure 1.** (a) Schematic view of a cell with a charged helium surface. (b) A picture of a liquid 'border' at the helium surface along the charged boundary [38].

to the liquid surface, the origin of coordinates lies on the surface of the unperturbed liquid, and the interval $z < 0$ corresponds to the liquid phase.

The electric fields $E_-$ and $E_+$ above and below, respectively, the helium surface charged with density $n_s$ have the form

$$E_- = \frac{V}{h} - 4\pi\sigma\,\frac{d}{h}\,, \tag{2.1}$$

$$E_+ = \frac{V}{h} + 4\pi\sigma\,\frac{h-d}{h}\,, \tag{2.2}$$

where the surface charge density $\sigma = en_s$, and $V$ is the potential difference between the plates of a cell (Fig. 1a).

When helium is completely shielded against the external field ($E_- = 0$), the quantity

$$E_+ = \frac{V}{d}\,. \tag{2.3}$$

At given $V$ and helium film thickness $d_0$ in the absence of an external field, the helium surface bends under the action of electron pressure (the case of $E_- = 0$) $P_{el} = E_+^2/8\pi$ to the depth

$$\xi_0 = d - d_0\,, \tag{2.4}$$

depending on the conditions of mechanical equilibrium and preservation of the total liquid volume:

$$\rho g\xi_0 + \frac{V^2}{8\pi d_0^2} = \rho g\xi_\infty\,, \tag{2.5}$$

$$L^2\xi_0 + (L_0^2 - L^2)\xi_\infty = 0\,, \quad L_0 > L\,, \quad |\xi_\infty| \ll d\,. \tag{2.6}$$

Here, $\rho$ is the liquid helium density, $g$ is the acceleration of gravity, $L$ is the electron disk radius at the helium surface, $L_0$ and $\xi_\infty$ are the liquid surface radius and deformation, respectively, outside the electron disk. Condition (2.5) is fulfilled if

$$\kappa^{-1} \ll L\,, \quad \kappa^{-1} \ll L_0 - L\,, \quad \kappa^2 = \frac{\rho g}{\alpha}\,, \tag{2.7}$$

where $\alpha$ is the surface tension coefficient, and $\kappa$ is the capillary constant. Finding $\xi_\infty$ from formula (2.6), namely

$$\xi_\infty = -\frac{\xi_0 L^2}{L_0^2 - L^2}\,,$$

and substituting it into formula (2.5) lead to

$$\xi_0 = -\frac{V^2}{8\pi\rho g^* d_0^2}\,, \qquad g^* = g\left(1 + \frac{L^2}{L_0^2 - L^2}\right). \tag{2.8}$$

A film is considered thick (a semiinfinite problem) if

$$\kappa d \gg 1\,. \tag{2.9}$$

In this case, the equilibrium and dynamic properties of a charged liquid surface do not depend on $d_0$ or the degree of its deformation (2.8), although such an effect always accompanies the appearance of electrons on this surface. By way of example, Fig. 1b presents the overall picture of a charged 'mirror' [38].

It should be noted that deformation effects are intrinsic in problems with charges on the helium surface. Also of interest, besides deformation on $L$ scales (Fig. 1a), are events featuring capillary constant $\kappa$ (including those in the reconstruction problem) and the formation of Coulomb ordering in a system of charges at distances $r_s$ satisfying the condition $r_s\sqrt{n_s} \approx 1$.

### 2.2 Instability of a charged liquid surface

The problem of stability loss for a bulk charged liquid surface is a necessary introduction to the nonlinear phenomena considered below. The essence of the problem was discussed from different standpoints in Refs [2–6] (see also papers [39–41]). A review of the known calculations facilitates the choice of adequate terminology and notions, such as maximum fields and densities, the degree of occupation (charging state) $\nu$ of a free liquid surface, and the relationship between $\nu$ and external fields [see relations (2.16) below]. In what follows, dynamic information is considered along with a fluctuational scenario of the development of instability (an analogy with first-order phase transitions).

**2.2.1 Dynamic instability scenario.** The dynamic behavior of a charged surface of the bulk liquid in the region far away from characteristic 2D plasma frequencies is described by the set of equations

$$\begin{aligned}
&E_{+\mathrm{t}}\big|_{z=\xi(x,y)} + E_{-\mathrm{t}}\big|_{z=\xi(x,y)} = 0\,,\\
&v_z\big|_{z=\xi(x,y)} = \frac{\partial\xi}{\partial t} + \mathbf{v}\nabla\xi\,,\\
&-\rho g\xi - \frac{\partial\Phi}{\partial t} - \frac{1}{2}\,\rho v^2 + \frac{1}{8\pi}\left(E_{+\mathrm{n}}^2 - E_{-\mathrm{n}}^2\right)\Big|_{z=\xi(x,y)}\\
&\qquad = \alpha\left(\frac{1}{R_1} + \frac{1}{R_2}\right),
\end{aligned} \tag{2.10}$$

where $\xi(x, y, t)$ is the deflection of the surface from the equilibrium flat shape, $\alpha$ is the surface tension of liquid helium, $\rho$ is its density, $R_1$ and $R_2$ are the principal radii of curvature at a given point of the deformed surface, $\mathbf{v} = \nabla\Phi$, $\Phi$ is the velocity potential in helium, $\mathbf{E}_\pm = -\nabla\varphi_\pm$ is the electric field strength, $E_{\pm\mathrm{t}}$ and $E_{\pm\mathrm{n}}$ are its tangential and normal components, and the potentials $\Phi$ and $\varphi$ satisfy the Laplace equation.

The linear variant of equations (2.10) leads to the dispersion law for small oscillations of a charged liquid surfaces (Gor'kov and Chernikova [36]):

$$\omega^2 = \frac{k}{\rho}\left(\rho g + \alpha k^2 - k\,\frac{E_+^2 + E_-^2}{4\pi}\right). \tag{2.11}$$

If at the same time $E_- = 0$, the problem reduces to that discussed in Landau's and Lifshitz's course [2]:

$$\omega^2 = \frac{k}{\rho}\left(\rho g + \alpha k^2 - k\,\frac{E_+^2}{4\pi}\right). \tag{2.12}$$

It follows from the conditions

$$\omega(k) = 0\,, \qquad \frac{\partial\omega^2}{\partial k} = 0 \tag{2.13}$$

that the critical strength squared of an external electric field equals

$$E_\mathrm{c}^2 = E_{+\mathrm{c}}^2 + E_{-\mathrm{c}}^2 = 8\pi\sqrt{\alpha\rho g}\,. \tag{2.14}$$

The critical uniform surface charge density is given by the relation

$$(n_\mathrm{s}^{\max})^2 = \frac{\sqrt{\alpha\rho g}}{2\pi e^2}\,, \tag{2.15}$$

where $e$ is the electron charge.

The evidence of developing instability at a charged helium surface was first observed by Volodin et al. [40]. Leiderer [41] explored the dispersion law in the case of oscillations excited at the interface of a layer-separated superfluid $He^3-He^4$ solution charged with ions having different signs (the nature of the charges at the liquid interface is actually unessential but an important point is that they possess high enough mobility in moving along the interface). Figure 2 borrowed from this

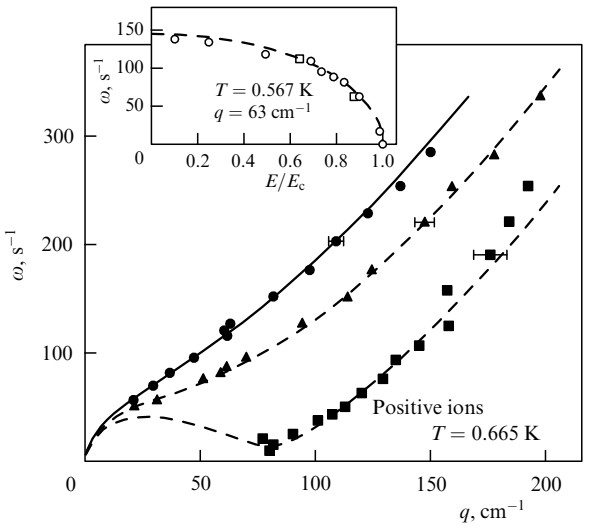


**Figure 2.** Dispersion relation for charged ripplons at the interface of a phase-separated $He^3-He^4$ mixture. The results of calculations using expression (2.12): solid curve for $E/E_\mathrm{c} = 0$, upper dashed curve for $E/E_\mathrm{c} = 0.71$, and lower dashed curve for $E/E_\mathrm{c} = 0.99$. Experimental data [41] for positive ions at $E/E_\mathrm{c} = 0.12$ (circles), $E/E_\mathrm{c} = 0.71$ (triangles), and $E = E_\mathrm{c}$ (squares). Inset: frequency corresponding to the wave vector $q = \kappa$ depending on the electric field strength [41]. Dashed curve — theoretical calculations using expression (2.12); squares and circles — experimental data for positive and negative ions, respectively.

study shows the experimentally found dispersion curve $\omega(q)$ of charged interface oscillations at $E_- = 0$ and its agreement with the theoretical prediction represented by formula (2.12). The inset illustrates details of the behavior of $\omega(q)$ in a dimple versus theoretical findings. Figure 2 demonstrates a fairly good agreement between theory and experiment.

In the general case, $E_- \neq 0$, the problem of charged helium surface stability becomes especially challenging. This variant is impossible to realize in well-conducting liquids where always $E_- = 0$ (complete screening), whereas in the case of charges above helium there is a whole continuum of states with $0 \leqslant E_- \leqslant V/h$.

Using the definitions (2.1), (2.2) and dimensionless quantities

$$\varepsilon_\pm = \frac{E_\pm}{4\pi\sigma_{\max}}\,, \qquad \sigma_{\max} = en^{\max}\,, \qquad \nu = \frac{\sigma}{\sigma_{\max}} \tag{2.16}$$

[$n^{\max}$ is defined by formula (2.15)], the general expression for $E_c^2$ (2.14) can be reduced to

$$\nu^2 + (\nu + 2\varepsilon_-)^2 = 2\,. \tag{2.17}$$

As $\varepsilon_- \to 0$, in accordance with the last relation, one finds

$$\nu(\varepsilon_- \to 0) \to 1\,. \tag{2.18}$$

In the opposite limit, $\nu \to 0$, it is easy to verify that

$$\varepsilon_-(\nu \to 0) = \varepsilon_+(\nu \to 0) \to \frac{1}{\sqrt{2}}\,. \tag{2.19}$$

The last result for $\pm\varepsilon$ is nonphysical (electron density tends to vanish, while the surface loses stability without any apparent reason).

The location of points (2.18), (2.19) in the plane $(\varepsilon_-, \nu)$ corresponds to the limiting values of function $\nu(\varepsilon_-)$ depicted in Fig. 3. The plot of function $\nu(\varepsilon_-)$ may be referred to as a phase diagram of charged helium surface stability.

Actually, limit (2.19) for dependence (2.17) has no real sense because the electrical equipotentiality condition for the deformed helium surface is no longer satisfied in passing to this limit:

$$\varphi = \text{const}\,. \tag{2.20}$$

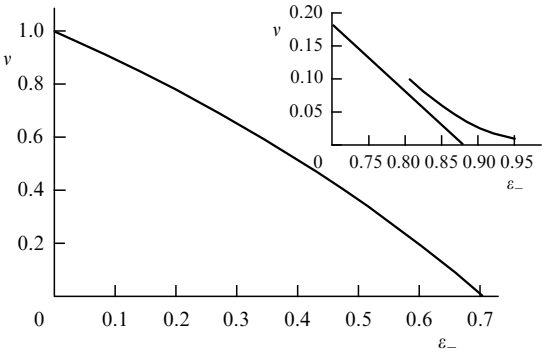


**Figure 3.** Phase diagram describing, in accordance with expression (2.17), a region of stability at the charged liquid surface in the dynamic (spinodal) scenario of its development in plane $(\varepsilon_-, \nu)$. The inner part of the diagram corresponds to the stable state. The inset shows the relative position of the binodal (practically straight line) and spinodal at low electron concentrations [42]. The advantage of the appearance of 'binodal' dimples in this region of $\nu$ is evident.

This requirement used to solve problems (2.11), (2.12) in the limit of small $\nu$ must be substituted by a more general condition

$$\mu = e\varphi + \zeta = \text{const}\,, \tag{2.21}$$

where $\zeta$ is the chemical part in the general definition (2.21) of the electrochemical potential $\mu$ of 2D charges above helium.

The structure of $\zeta$ for a system of electrons with finite number density $n_s$ is a self-contained problem having no accurate analytical solution. In what follows, we rely only on qualitative arguments and bear in mind the small electron density limit, which makes it possible to use the explicit form of $\zeta$ for an ideal gas:

$$\zeta = -T \ln \frac{n_T}{n(x)}\,, \qquad n_T = \frac{mT}{2\pi\hbar^2}\,, \qquad \frac{n_T}{n(x)} \gg 1\,. \tag{2.22}$$

Here, $T$ is the electron temperature coinciding below with liquid substrate temperature, $m$ is the effective charge mass, and $n(x)$ is the local electron density.

In the problem of charged helium surface equilibrium, the main part of condition (2.21) containing a large logarithm enters the system of equations defining the bulk equilibrium of an unperturbed 'electrons + flat liquid boundary' system. Relevant calculations [43] yield information on the quasifree electron distribution above the charged helium surface. As far as the stability problem is concerned, only addition $\delta\zeta(x)$, namely

$$\delta\zeta = T\,\frac{\delta n(x,t)}{n_s}\,, \qquad \frac{\delta n(x,t)}{n_s} \ll 1\,, \tag{2.23}$$

arising upon deformation of the liquid boundary, is of importance.

The use of linearized relation (2.21), (2.23), and standard operations employed to calculate the dispersion law for a charged liquid surface leads to the result [42]

$$\frac{\rho\omega^2}{\alpha} = (\kappa^2 - \eta^2)q + q^3\,, \qquad \eta^2 = \frac{n_s e^2 E_+^2}{\alpha T}\,. \tag{2.24}$$

It is easy to see that dispersion law (2.24) as $\eta^2 \to 0$ goes over to correct asymptotics $\omega(q)$ without participation of Coulomb forces.

Oscillations with dispersion law (2.24) lose stability, as they do in the Frenkel–Tonks problem. But the loss takes place in a region other than that corresponding to Eqn (2.14), where

$$\eta^2 > \kappa^2\,, \qquad E_+ \approx E_- \approx \frac{V}{h}\,. \tag{2.25}$$

Characteristic density $n_s^c$ discriminating between two limiting cases of shielding is found from the estimate

$$\frac{2\pi e^2 n_s^c}{qT} \simeq 1\,,$$

where $q$ is the characteristic wave number of perturbation $\xi(x)$. For the wave numbers of the same order as the capillary length and temperatures on the order of 1 K, this density has the following scale: $n_s^c \simeq 10^4 - 10^5$ cm$^{-2}$.

It follows from Eqn (2.25) that a field growing with decreasing $n_s$ as $\varepsilon_- \propto \nu^{-1/2}$ needs to be used in order to

reach the instability of a weakly charged helium surface. This inference qualitatively differs from 'equipotential' predictions [see asymptotics (2.19)]. This means that dynamic stability in the region of small $v$ is not restricted to point (2.19) but extends as $\propto v^{-1/2}$ up to $\varepsilon_- \to \infty$ [42].

Consideration of formulas (2.17)–(2.25) and Fig. 3 paves the way for an analysis of the reconstruction of a charged helium surface in terms of the phase transition theory. The dynamic boundary of stability has much in common with the spinodal in two-component separation dynamics. The role of concentration is played by $v$, and that of temperature by field $E_-$. Therefore, an alternative binodal scenario of transition becomes possible if multicharged dimples are introduced into the consideration [42].

**2.2.2 Fluctuational instability scenario.** Fluctuational binodal development of instability is associated with the possibility of forming multicharged clusters (dimples) with a finite electron (ion) charge localized in their nuclei on a flat charged helium surface. The process of formation of a single multielectron dimple can be at first presented semianalytically without regard for the details of electron distribution $n(r)$ in its central part. Simplification reduces to the choice of function $n(r)$ in the following model form:

$$n(r) = \frac{N}{\pi R^2} \exp\left(-\frac{r^2}{R^2}\right), \tag{2.26}$$

where $N$ is the total number of electrons in a dimple, which constitutes the external parameter of the problem, and $R$ is the variational parameter having the sense of a charged spot radius.

The expression for the excess energy of a 'dimple + self-consistent deformation of helium surface' system for $\nabla\xi \ll 1$ may be written (Shikin, Leiderer [44, 45]) as

$$W = \int \mathrm{d}^2 r \left[\frac{\alpha}{2}\left[(\nabla\xi)^2 + \kappa^2\xi^2\right] + eE_\perp n(r)\xi + e^2 \int \mathrm{d}^2 r' \, \frac{n(r)\, n(r')}{|\mathbf{r} - \mathbf{r}'|}\right], \tag{2.27}$$

where $\xi(r)$, $\rho$, $\alpha$, $g$, and $\kappa$ were defined above. The term $(\nabla\xi)^2 + \kappa^2\xi^2$ takes account of the deformation contribution to energy $W$, while term $eE_\perp n(r)\xi$ characterizes the interplay between deformation and electron parts of the problem, and the last term written in the integral form stands for the total energy of Coulomb interaction among electrons concentrated in a flat spot of radius $R$.

Taking advantage of the explicit form of the electron distribution $n(r)$ (2.26), the expression for $W$ (2.27) can be transformed into

$$W = \frac{Q^2 E_\perp^2}{8\pi\alpha} \exp\left(\frac{\kappa^2 R^2}{2}\right) \mathrm{Ei}\left(-\frac{\kappa^2 R^2}{2}\right) + V_\mathrm{C}(R), \tag{2.28}$$

$$V_\mathrm{C}(R) = \frac{C_0 Q^2}{R}, \qquad Q = eN, \tag{2.29}$$

where $\mathrm{Ei}\,(y) = \int_{-\infty}^{y} \mathrm{d}t(\exp t)/t$ is the integral exponential function. For distribution (2.26), $C_0 = 1/2(\pi/2)^{1/2}$. The value of $R$ is found from the condition $\partial W/\partial R = 0$.

An analysis of the extreme properties of $W(r)$ (2.28) brings us to the conclusion that a stable solution of the equation $\partial W/\partial R = 0$ in $R$ is feasible only under the condition

$$\kappa R < 1. \tag{2.30}$$

In the limiting case $\kappa R \ll 1$, the value of $R$ and the total energy $W$ assume the form

$$R = R^* = C_0 \frac{4\pi\alpha}{E_\perp^2}, \qquad \xi(0) = -\frac{QE_\perp}{2\pi\alpha} \ln\frac{1}{\kappa R^*}, \qquad W = -\frac{Q^2 E_\perp^2}{4\pi\alpha}\left(\ln\frac{C_1}{\kappa R^*} - 1\right), \qquad C_1 \approx 1. \tag{2.31}$$

An interesting result following from Eqn (2.31) is the $Q$-independence of $R^*$. Naturally, it would seem that $R^*$ will grow as Coulomb interaction in the charged dimple core increases with increasing $Q$. However, deformation forces that hold electrons in the dimple grow at the same rate, which makes the value of $R^*$ determined by the competition of these two factors independent of $Q$.

It is equally appropriate to comment on the quadratic dependence of energy $W$ (2.31) on $E_\perp$ and $Q$. The independence of deformation results of the $E_\perp$ direction has been mentioned before (see the dispersion law in Fig. 2 with the structure independent of the charge sign). As regards dimples, the sign of field $E_\perp$ is implied such that charges with a given sign are driven to the center of the dimple. On changing the sign of $E_\perp$, the same procedure has to be undertaken for the sign of charge. Otherwise the dimple will not be formed.

Asymptotics (2.31) in the vicinity of $\kappa R \leqslant 1$ become inexact, which necessitates the use of numerical methods to determine the corresponding quantities. To this effect, it is convenient to present energy (2.28) in the dimensionless form

$$\tilde{W} = 2\left(\frac{2}{\pi}\right)^{1/2} \frac{W}{Q^2\kappa} = s \exp\left(\frac{x^2}{2}\right) \mathrm{Ei}\left(-\frac{x^2}{2}\right) + \frac{1}{x}, \tag{2.32}$$

where

$$s = \frac{1}{2\kappa R^*}, \qquad x = \kappa R. \tag{2.33}$$

Setting $s$ and constructing function $\tilde{W}(s, x)$, one can find the value and position of its minimum. This information is sufficient to examine the properties of $\tilde{W}$ and $R$ in the vicinity of $\kappa R \leqslant 1$. For example, the minimum of function $\tilde{W}$ appears for the first time when $s = s_{\min} = 0.9$ at point $x_{\max} = 1.14$. Function $\tilde{W}$ first vanishes when $s = s_* = 1.05$ at point $x_* = 0.72$. The dependence of $x$ on parameter $1/2s = \kappa R^*$ in the region $s \geqslant s_{\min}$ shown in the left inset to Fig. 4 gives the value of the real dimensionless dimple radius $x$ versus its asymptotic value $\kappa R^*$.

Relations (2.26)–(2.32) are sufficient to determine conditions for the appearance of dimples. Clearly, there is competition between the dimple energy and the electrostatic energy of the capacitor with 2D electrons in which the dimple formed fluctuationally. The uncertainty lies in the estimation of an optimal charge giving rise to a critical dimple. However, the amount of this charge has no effect on the critical field. This linear approach seems acceptable in order to consider dimples as candidate structures responsible for the fluctuational development of instability.

A more careful variational calculation of the parameters of a multielectron dimple reported by Mel'nikov and Meshkov [24, 25] has demonstrated that electron number

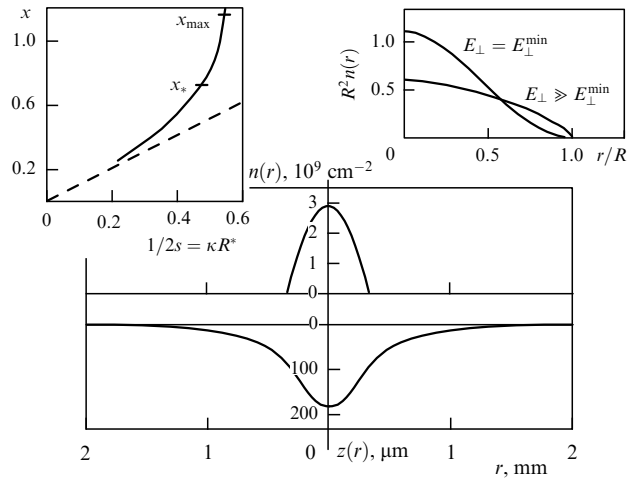


**Figure 4.** The structure of an individual dimple [28] at a fixed total electron charge. Left inset shows the dependence of radius $x$ on $1/2s$ (holding field) that clarifies details of the energy behavior (2.32). Right inset displays the electron density in the dimple calculated in Refs [24, 25] at different supracriticality values. The profile with $E_\perp = E_\perp^{min}$ corresponds to the situation in the vicinity of the critical field for dimple appearance; the variant with $E_\perp \gg E_\perp^{min}$ is appropriate to a well-formed dimple far from $E_\perp = E_\perp^{min}$.

density monotonically decreases with the distance from the dimple center and tends to zero as $\sim (1 - r^2/R^2)^{1/2}$, $r \to R$ in the limit of $\kappa R \ll 1$ at the edge of the electron spot. The $n(r)$ distribution in the $\kappa R \leqslant 1$ region is close to Gaussian. The results of numerical calculations of function $n(r)$ from papers [24, 25] illustrating the behavior of local electron density in different limiting cases give the dependences shown in the right inset to Fig. 4. As for the averaged characteristics of a dimple, e.g., the minimal field strength $E_\perp^{min}$ making possible the existence of an individual multielectron dimple, they are close to those in Ref. [44]. A criterion for energy-related advantage of dimple formation is the requirement of $s > s_*$ from which it is possible to derive (see above)

$$E_\perp \geqslant E_\perp^{min}, \qquad (E_\perp^{min})^2 = (2\pi)^{3/2} s_* \kappa\alpha = (16.520 \pm 0.005)\kappa\alpha . \tag{2.34}$$

For example, it follows from Refs [24, 25] that field $E_\perp^{min} = 4.06(\kappa\alpha)^{1/2}$, in excellent agreement with formula (2.34).

By way of illustration, Fig. 4 shows the direct 'portrait' of an individual dimple from Ref. [28].

With the two scenarios of instability development in hand, one may try to construct a phase diagram for decay of the flat charged liquid state even at this stage. However, the long-range character of Coulomb interaction hinders this operation at the linear level and does not permit avoiding a number of uncertainties. The main of them is the number of electrons entering an individual dimple upon corrugation of the liquid surface. Additional information about the details of instability development is needed to eliminate the uncertainties.

### 2.3 Development of instability

A. The initial stage of instability development is of importance for several reasons. First, it gives an idea of real small parameters necessary to construct a nonlinear perturbation theory. Second, continuity breaks in the charge distribution over the corrugated liquid boundary naturally start to be detected at this stage, being essential for subsequent consideration. Finally, the mechanism of 'triggering' the decay of the flat charged liquid state is as interesting in itself as in traditional spinodal scenarios.

Using the parameter

$$\Delta = \frac{E_+^2 + E_-^2}{E_c^2} - 1 , \tag{2.35}$$

which characterizes the proximity of a system to the stability threshold, and quantity

$$v_* = \frac{E_+^2 - E^2}{E_c^2} = v(2\varepsilon_- + v) \tag{2.36}$$

[here, $E_-$ and $E_+$ are defined in formulas (2.1),(2.2), $v$ is from Eqn (2.16), and $E_c$ is from Eqn (2.14)] proportional to the unperturbed electron surface density, and assuming $|\Delta| \ll 1$ and $v_* \ll 1$, one can present the one-dimensional solution of the initial system of equations (2.10) in the form [18]

$$\xi(\mathbf{r}) = \frac{a}{2}\left[\chi(x,t)\exp(\mathrm{i}kx) + \text{c.c.}\right], \qquad a = k^{-1} = \left(\frac{\alpha}{\rho g}\right)^{1/2} . \tag{2.37}$$

The amplitude of $\xi$ is small compared with the capillary length. The authors of Ref. [18] expanded all the equations of system (2.10) up to third-order terms in $\chi \sim \xi/a$ and thereby obtained the equation for the perturbation amplitude $\chi$:

$$\frac{1}{gk_0}\ddot{\chi} = -\frac{(k-k_0)^2}{k_0^2}\chi + \frac{1}{2k_0^2}\frac{\partial^2\omega^2}{\partial k^2}\frac{\partial^2\chi}{\partial x^2} + 2\mathrm{i}\omega\frac{\partial\omega}{\partial k}\frac{\partial\chi}{\partial x} + 2\Delta\chi + \left[8(v_*^2 - 1) + \frac{11}{2}\right]\frac{|\chi|^2\chi}{4} . \tag{2.38}$$

Formally, manipulations (2.35)–(2.38) are inherent in all calculations of reconstruction processes in the framework of the aforementioned 'uniform' approximation [14, 19]. For a charged helium surface, this means conservation of the equipotentiality of the curved boundary that takes place at least at the initial stage of the decay.

Transformation (2.37) shifts the origin of counting in $k$-space to point $k = k_0$. Therefore, the amplitude $\chi(x,t)$ in the vicinity of the critical point is a function weakly dependent on coordinate $x$. The proximity to the threshold means that $(k-k_0)^2/k_0^2 \ll 1$ and $\partial\omega/\partial k \ll 1$; hence, the appropriate terms in Eqn (2.38) can be neglected. The remaining right-hand side of equation (2.38) in a homogeneous case ($\partial\chi/\partial x = 0$) ensues from variation of the potential

$$V(\chi) = -2\Delta|\chi|^2 - \left[8(v_*^2 - 1) + \frac{11}{2}\right]\frac{|\chi|^4}{8} . \tag{2.39}$$

At small enough $v_*$, the potential $V(\chi)$ has a minimum, and the system must pass into this state if the terms describing dissipation effects are inserted into equation (2.38). In the limit $v_* \to 0$, the stationary corrugation amplitude $\chi_0$ has the form

$$\chi_0^2 = \frac{16\Delta}{5} . \tag{2.40}$$

Such a type of $\chi_0$ behavior (reconstruction begins only in the region $\Delta > 0$, and amplitude $\chi_0$ monotonically increases with increasing $\Delta$) is usually called a soft-type transition

(reconstruction) following Landau [46], and Zaitsev and Shliomis [14]. The coincidence is not surprising bearing in mind the homogeneous nature of relations (2.35)–(2.38).There is no soft-type one-dimensional solution in the region $v_*^2 > 5/16$.

For charged liquid media such 'one-dimensional' transition is purely academic because, on the whole (i.e., over the entire time interval up to the instant of establishing equilibrium), it is symmetrically and energetically less advantageous than two-dimensional reconstruction scenarios. Nevertheless, the one-dimensional corrugation pattern may prevail at the beginning of the process until the nonlinear terms of equation (2.39) get involved. As experience shows, the corrugation forms first and foremost along the natural borders of a 2D system, regardless of the degree of its average population. Evidently, the initial corrugation reproducing smooth boundary geometry is essentially one-dimensional. Details of such boundary reconstruction remain to be elucidated.

2D corrugation is energetically more advantageous far away from the boundaries and at a large enough time interval from the initial stage of the process. According to papers [17, 19], there is a symmetric hexagonal structure characterized by three wave vectors oriented at a 60° angle with respect to each other. In this case, the expression for energy $V(\chi)$ contains new qualitatively important negative terms of the third order in the amplitude; eventually, it gives a lower equilibrium energy compared with that in a system of stripes or a square lattice. Instead of potential (2.39), the result is

$$V(\chi_0) = \frac{3}{2}\,\gamma\chi_0^4 + 3v_*\chi_0^3 - 6\Delta\chi_0^2\,, \qquad \gamma \approx 0{,}96\,. \tag{2.41}$$

Expression (2.41), unlike formula (2.39), does not contain terms of order $v_*^2\chi_0^4$. Function $V(\chi_0)$ (2.41) reaches a minimum at

$$\chi_0 = -\left(\frac{3v_*}{4\gamma} + \sqrt{\frac{2\Delta}{\gamma} + \frac{9v_*^2}{16\gamma^2}}\right). \tag{2.42}$$

In the limit $\Delta \to 0$, the last formula yields

$$\chi_0 = -\frac{3}{2}\,\frac{v_*}{\gamma}\,, \tag{2.43}$$

i.e., there is a transition as in the case (2.39), but (using the terminology of Refs [14, 19, 46]) it occurs in the hard regime with finite $\chi_0$ values as $\Delta \to 0$.

It should be noted that manipulations with parameter $\Delta$ (2.35) are feasible only for liquid boundaries with a variable density of mobile charges at the interface. When there is complete shielding of the field, so that either $E_+$ or $E_-$ vanishes, such a degree of freedom is absent. Indeed, for metals one finds

$$v_*^{\mathrm{m}} = \frac{E_+^2}{E_{\mathrm{c}}^2}\,. \tag{2.44}$$

Quantity $v_*^{\mathrm{m}}$ (2.44) can be small if $E_+ \ll E_{\mathrm{c}}$. In this case, however, a metallic liquid is stable. If $E_+ \to E_{\mathrm{c}}$, $v_*^{\mathrm{m}}$ tends to unity.

B. The above results (2.40), (2.43) give a clear idea of the small parameters needed to develop a nonlinear perturbation theory [14, 17, 19]. What is meant are the conditions

$$\Delta \ll 1\,, \qquad v_* \ll 1\,, \tag{2.45}$$

violation of which reduces the theory to qualitative assertions. However, the list of necessary limitations is wider than that. Mel'nikov and Meshkov [23–25] were the first to observe that, in terms natural for a problem with surface charges, the total charge density $\tilde{v} + v_*$ during reconstruction under the equipotential scenario cannot vanish:

$$\tilde{v} + v_* > 0\,. \tag{2.46}$$

From this standpoint, the variant of reconstruction (2.40) for $v_* \to 0$ and $\Delta \neq 0$ makes no sense whatever.

The assessment is even more difficult in a hard regime. Nevertheless, calculations made by the authors of Refs [23–25] suggest violation of requirement (2.46) in the parameter region preceding the establishment of equilibrium corrugation. The results of these calculations are presented in Fig. 5. In the general case, the energy $\varepsilon$ of the corrugated boundary depends on two variables: corrugation amplitude $\xi$, and modulated charge density $\tilde{v}$. Variation of $\varepsilon(\xi, \tilde{v})$ in one of these variables gives the relationship between $\xi$ and $\tilde{v}$ at an arbitrary stage of adjustment (the electron part of the problem undergoes rapid adjustment to the arbitrary deformation $\xi$). The second variation determines the energy extremum position in which the reconstructed boundary is located. Figure 5 gives an idea of the value of $\varepsilon(\tilde{v}, \xi(\tilde{v}))$ at intermediate stages of corrugation for different values of supercriticality $\Delta$, including its negative part. The feasibility of criterion (2.46) is indicated by the dashed straight line.

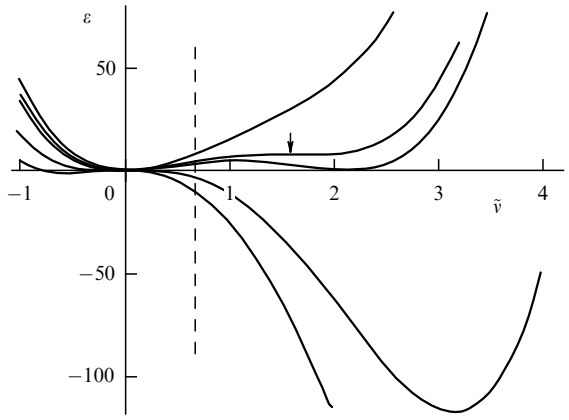


**Figure 5.** Intermediate deformation energy $\varepsilon$ as a function of $\tilde{v}$ for different values of supercriticality. Dashed straight line marks the boundary of violation of condition (2.46).

It follows from Fig. 5 that condition (2.46) is violated before the system has had time to exponentially reconstruct. This means that calculation of the final reconstruction stage in the equipotential scenario ceases to be valid. The total charge being fixed, its distribution along the boundary loses uniformity. Is there an alternative? Yes, there is insofar as prerequisites exist for the formation of a system of multicharged dimples, the notion of which was introduced in Section 2.2.

C. Concluding the discussion of the initial reconstruction stage, one cannot overpass the problem of boundary conditions for equation (2.38). This detail is actually

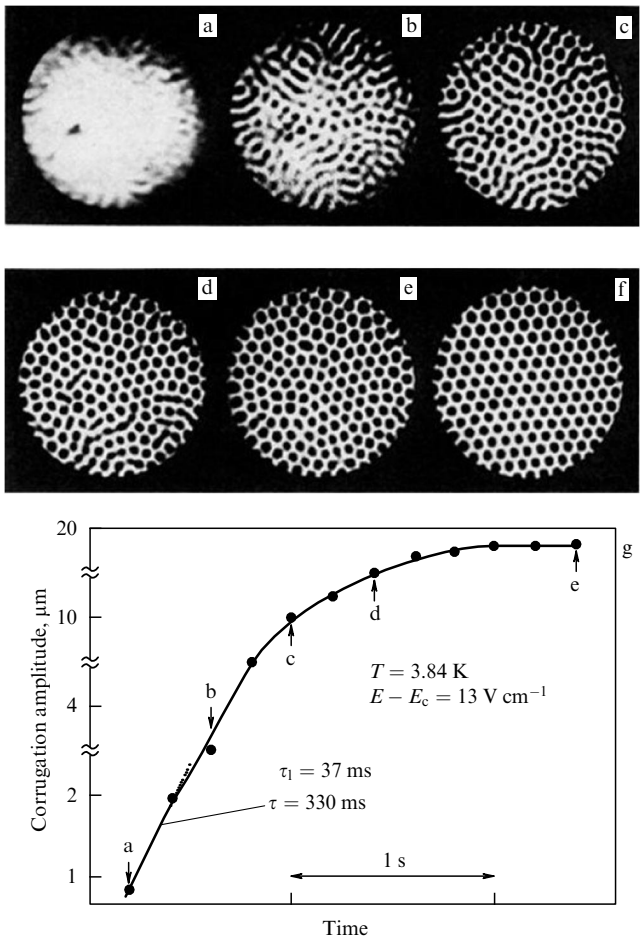


**Figure 6.** (a–f) Corrugation evolution with time under conditions of maximum occupation of a helium surface by electrons. (g) Time-dependent corrugation amplitude [26, 27]. Time $\tau_l$ is defined by formula (2.47), and $\tau$ is the total estimated time of instability development at a given degree of supercriticality. The authors of Refs [26, 27] argue that prefinal states (d, e) of the corrugated mirror have a glass-like structure. 'Annealing' using a small-amplitude oscillating field brings the dimples together to give rise to a honeycomb structure (f).

beyond the framework of the existing publications concerned with stability. However, it is indispensable to 'trigger' the decay (as is well known from an essentially similar problem of spinodal decay in the theory of first-order phase transitions [47]).

The data of Fig. 6 [26, 27] give evidence that equation (2.38) in the region linear in $\zeta$ makes sense within a wide range of $v$ values. The estimate of time $\tau_l$, namely

$$\tau_l^{-1} = \sqrt{\frac{2\pi\alpha}{g}(E^2 - E_c^2)}\,, \tag{2.47}$$

gives its correct scale. The figure displays a well-apparent 'watershed' between the spinodal and FT scenarios of developing instability. As for the mechanism of triggering instability, the question of whether it is underlain by equilibrium surface shape fluctuations stimulated by Langevin forces or by instrumental effects remains to be clarified.

### 2.4 Reconstruction of a charged helium surface

The analysis of the initial stage of instability development in Section 2.3 gives evidence that the final (metastable) reconstructed liquid surface must have a 'dimpled' (nonequipotential) structure. Its details are discussed below for two qualitatively interesting $v$-limit cases:

(a) low population, $v \ll 1$. In this limit, there is every reason to speak about the binodal variant of the development of events;

(b) the reconstruction scenario with maximum filling of the surface with charges ($v \leqslant 1$), which is pertinent to refer as a 'mixed' one.

**2.4.1 Small-$v$ region.** As noted in Section 2.2, the 'spinodal' critical field in the small-$v$ region increases as $v^{-1/2}$ [see formula (2.25) and Fig. 3]. Let us show that binodal dimple formation in this region requires finite $\varepsilon_-$ values.

Transition from the flat to the corrugated state is governed by competition between the electrostatic energy $V_C$ of the capacitor with 2D electrons filling the entire available liquid surface and the total energy $nW_n$ of the system of $n$ dimples containing the same total charge $Q$. The problem of comparison contains an uncertainty because, in the general case, the charge of an individual fluctuationally formed dimple and the charge distribution over the totality of dimples are poorly defined. The situation only simplifies in the limiting case of $v \ll 1$, where all free electrons draw together in one multicharged dimple (in this case, the flaw in reasoning is compensated for by references to experiments in which events proceeded as described).

The Coulomb energy $V_C$ of an electron system with a total charge $Q$ in the region bounded by a circle of radius $L$ between capacitor plates (see Fig. 1) has the scale

$$V_C = Q^2\,\frac{(h-d)d}{L^2 h}\,, \qquad Q = \pi L^2 e n_s\,. \tag{2.48}$$

The structure of energy $W$ for a single dimple was discussed in Section 2.2 [see formula (2.32)]. For comparison with $V_C$ concerned, it is possible to use the expansion of $W$ near the zero point $(s_0, x_0)$:

$$W(s_0, x_0) = 0\,, \qquad s_0 = 1.05\,, \qquad x_0 = 0.75\,,$$

$$W(s, x_0) \simeq \frac{\partial W}{\partial s_0}(s - s_0)\,.$$

As a result, the equality of the competing energies takes the form

$$Q^2\,\frac{(h-d)d}{L^2 h} = \frac{\partial W}{\partial s_0}(s_* - s_0)\,, \tag{2.49}$$

which gives the value of $s_*$.

The electric field $E_+^{\max}$ related to $s_*$ defines the abscissa on the plane $(v, \varepsilon_-)$ (in this region, $E_\perp = E_+ \simeq E_- = V/h$) where the binodal rests as $n_s \to 0$. These results complete the description of the transition region in which the flat charged surface is replaced by a surface with a dimple.

Thus, instability stimulated by the finite $V/h$ value in the limit $v \to 0$ leads to the appearance of a separate dimple 'collecting' all surface electrons, but not to periodic reconstruction (as predicted by the equipotential theory). This process can also end with the formation of several dimples randomly sharing the total surface charge among themselves. However, there are no common causes here for a periodic reconstruction involving the entire charged mirror.

It should be noted that two dimples separated by a finite distance may be in equilibrium. The interaction energy $W_{dd}$ between them contains both Coulomb and deformation

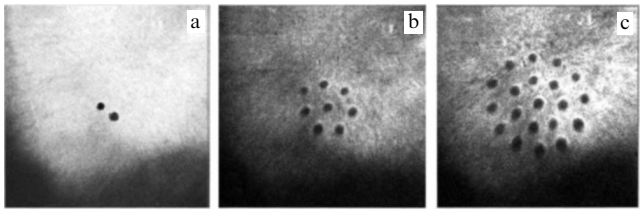


**Figure 7.** (a) Aperiodic reconstruction in the region of small $v$, and (b, c) increase in the number of dimples and the appearance of signs of honeycomb reconstruction with a rise in occupation $v$ of the helium surface with electrons.

parts:

$$W_{\rm dd}^{\rm b} = -\frac{Q^2 E_\perp^2}{2\pi\alpha} K_0(\kappa r) + \frac{Q^2}{r}\,. \tag{2.50}$$

Here (as above), $Q$ is the total charge of the dimple, $E_\perp$ is the holding field, $r$ is the distance between the dimples, and $K_0(x)$ is the modified Bessel function. Energy (2.50) goes through a minimum, $\partial W_{\rm dd}^{\rm b}/\partial r = 0$, at point $r_{\rm min}$ found from the equation

$$K_1(x_{\rm m}) - x_{\rm m}^{-2} = 0\,, \qquad x_{\rm m} = \kappa r_{\rm min}\,, \tag{2.51}$$

$$x_{\rm m} \geqslant 1\,. \tag{2.52}$$

The presence of metastable coupling (2.51) between dimples qualitatively explains why the totality of dimples formed during the decay of a 2D-charged system (Fig. 7) is collected in mesostructures having internal equidistance with a characteristic distance on the order of the capillary distance.

**2.4.2 Mixed scenario of reconstruction in the region $v \lesssim 1$.** In the opposite limiting case of $v \leqslant 1$, it is easy to determine the position of the spinodal in the graph $(v, E_-)$ (see Fig. 3). However, the alternative part of the problem of nucleation 'decay' of the flat charged state (binodal) remains uncertain for lack of a characteristic scale for the charge during the formation of the nucleus-dimple. At the same time, experimental data give unambiguous evidence of periodic reconstruction. The difficulties are obviated by turning to the temporal evolution of FT decay. As noted before [see comments on inequality (2.46) and Fig. 5], the spinodal scenario of decay for a fixed value of the total surface charge leads to the appearance of periodically arranged neutral spots on the charged liquid surface. This picture certainly corresponds to the end of spinodal and the onset of binodal evolution with well-defined initial conditions (the charge of a dimple is known, and all dimples are identical). The scenario with initial spinodal and subsequent binodal stages of charged liquid surface deformation is referred to as mixed. The main known factors related to FT decay in the $v \leqslant 1$ region qualitatively co-exist in the framework of this scenario, viz. periodicity of reconstruction, loss of equipotentiality along the corrugated liquid surface, and, as will be shown below, stepwise behavior of corrugation amplitude during formation of the stationary reconstructed state of the liquid boundary.

(1) Regarding the question of a corrugated surface state in the critical electric field $E_+^{\rm max}$ with charge

$$Q_0 \simeq 2aen_{\rm s}^{\rm max} \tag{2.53}$$

per dimple, it is necessary to make sure that the deformed helium surface can hold the critical charge (probably, in a nonlinear manner) and check the fulfillment of the inequality

$$\bar{W}(E_+^{\rm max}, Q) \geqslant \tilde{W}(E_+^{\rm max}, Q_0, b), \qquad E_+^{\rm max} = 4\pi e n_{\rm s}^{\rm max}\,, \tag{2.54}$$

where $n_{\rm s}^{\rm max} \equiv n^{\rm max}$ follows from Eqn (2.16), $\bar{W}(E_+^{\rm max}, Q)$ and $\tilde{W}(E_+^{\rm max}, Q_0, b)$ are the total energies of homogeneous and corrugated states of the helium surface, respectively, and $b$ is the lattice period, generally speaking different from the capillary length $a$. There is no reason to require the equality of energies in formula (2.54) because it is unrelated to a true binodal transition from the flat to the corrugated state. Nevertheless, it is desirable to have the energy $\tilde{W}(E_+^{\rm max}, Q_0, b)$ lower than $\bar{W}(E_+^{\rm max}, Q)$; otherwise, it is difficult to understand the general course of events.

In light of the aforesaid, the one-dimensional corrugation problem reduces to calculating the energy difference $\tilde{W}(E_+^{\rm max}, Q_0, b) - \bar{W}(E_+^{\rm max}, Q)$ [see Eqn (2.54)]. It should be noted that the one-dimensional scenario not only provides a convenient model but also describes the actually observed state of the corrugated surface [28]. Moreover, it is the least stable variant of corrugation. Laplace pressures stabilizing the picture here are half of what they are in two-dimensional scenario. The one-dimensional solution yields a lower bound for corrugation stability.

The primary functional for the one-dimensional periodic corrugation energy (per unit thread length) is given as follows:

$$\begin{aligned}\delta\tilde{W}(E_+^{\rm max}, R, a) &= \tilde{W}(E_+^{\rm max}, Q_0, a) - \bar{W}(E_+^{\rm max}, Q)\\ &= \int_{-a}^{+a} {\rm d}x \left[\frac{\alpha}{2}\left[(\nabla\xi)^2 + \kappa^2\xi^2\right] + eE_+^{\rm max}\delta n(x)\xi(x)\right] + \delta\langle W_{\rm C}(r)\rangle,\end{aligned} \tag{2.55}$$

$$\delta\langle W_{\rm C}(r)\rangle = 2e^2 n_{\rm s}^2 a^2 \ln\frac{a}{\pi R}\,,$$

$$\xi(x) = \zeta(x) - \langle\zeta\rangle\,, \quad \delta n(x) = n(x) - n_{\rm s}\,;$$

it is counted from the flat charged liquid surface energy and written for one lattice period. Its Coulomb part has the form [48]

$$\delta\langle W_{\rm C}(r)\rangle = \frac{Q^2}{2}\left(\frac{1}{\tilde{C}} - \frac{1}{\bar{C}}\right) > 0\,, \tag{2.56}$$

$$\bar{C} = \frac{S}{4\pi d}\,, \qquad \tilde{C} = \frac{S}{4\pi d + 4a\ln(a/\pi R)}\,, \tag{2.57}$$

where $S$ is the area of the capacitor, $R$ is the radius of an individual thread, and $2a$ is the corrugation period; charge density $n(x)$ in a periodic dimple system is split into separate stripes, each characterized by a certain density distribution (e.g., Gaussian) $n_0(x)$:

$$\begin{aligned} n(x) &= \sum_l n_0(x - 2la)\,, \quad n_0(x) = n_0\exp\left(-\frac{x^2}{R^2}\right),\\ n_0 &\simeq \frac{2n_{\rm s}a}{\sqrt{\pi}\,R}\,, \quad R \ll a\,,\end{aligned} \tag{2.58}$$

and normalization (2.53). Mean values are subtracted from the respective variables $\zeta(x)$, $n(x)$, taking into account the general structure of functional (2.55).

Energy (2.55) exhibits the standard structure for the theory of multicharged dimples. The deformation-related

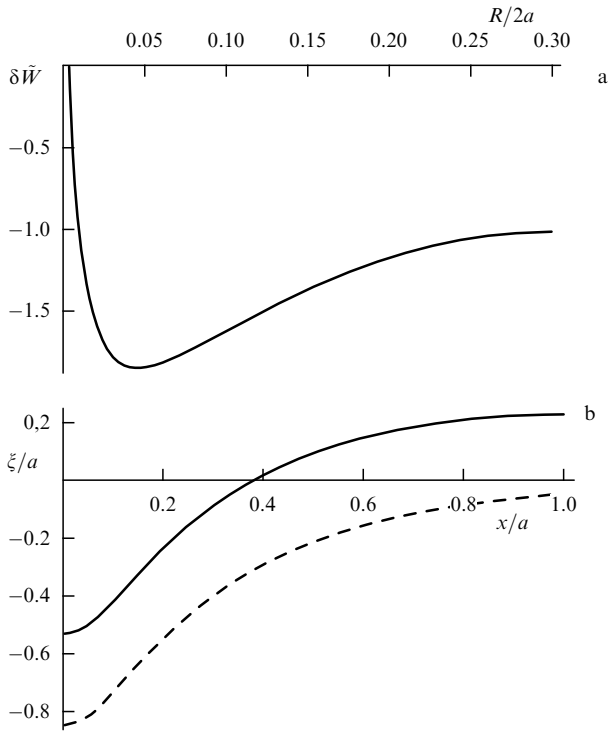


**Figure 8.** (a) Energy $\delta\tilde{W}$ of a one-dimensional dimple being a member of a periodic structure as a function of the electron spot radius. (b) One-dimensional dimple profiles: for a single free dimple (dashed line), and a periodic set of dimples (solid curve).

part represented by the terms in square brackets makes integrally the growth of deformation of the liquid surface under the action of local electron pressure energetically advantageous and accounts for the reduction in parameter $R/a$. The Coulomb component $\delta\langle W_C(r)\rangle$ hinders this process. The interplay between these factors results in the appearance of a negative minimum in the dependence $\delta\tilde{W}(E_+^{\max}, R/a)$ (2.55), which determines the equilibrium value of the parameter $R/a$. In order to obtain numerical values, it is necessary to find deformation $\xi(x)$ using $n(x)$ (2.58) from the equation for mechanical equilibrium of a liquid surface, calculate integrals (2.55) with the help of these distributions, and construct the dependence of energy (2.55) on the variable parameter $R/a$. This picture for external parameters corresponding to the case of $v = 1$ is presented in Fig. 8a [49]. The functional minimum reached at $R/a = 0.1$ is negative. In other words, the corrugated state is more energetically advantageous than the flat one.

Corrugation is stabilized in the region of $R/a \ll 1$, although the obtained numerical values should be regarded as rough estimates, bearing in mind that the values of $\nabla\xi(x) \leqslant 1$ are not parametrically small, as follows from data on the one-dimensional dimple deformation profile. These data are given in Fig. 8b together with the profile of an individual free dimple (for comparison). Obviously, the linear variant of the theory corresponding to the bilinear energy functional (2.55) needs to be quantitatively corrected [as follows from Fig. 8, the requirement $\nabla\xi(x) < 1$ used to derive expression (2.55) is met conditionally]. Nevertheless, the mixed scenario of reconstruction qualitatively appears to be self-consistent (reasoning from the assumption of continuity breaks in the equilibrium distribution of $n(x)$ leads to a final picture that confirms the initial provisions of the theory).

Moreover, it may be argued, based on details of the nonlinear solution [50] (not presented here), that the critical dimple depth $|\xi_0^{\max}| = 1.5a$ is not exceeded in the linear approach.

(2) *Honeycomb corrugation*. There are several reasons to additionally discuss the details of two-dimensional corrugation against the background of its one-dimensional realization. First, a reconstruction of this type most frequently occurs as dominant under practical conditions. Second, there is the issue of lattice choice (why honeycombs?). One more question raised in papers [23–25] concerns the details of charge distribution over a corrugated liquid surface. It may be a system of neutral islets against the conducting background (the model of Refs [23–25] or a version of 'soft' transition). An alternative is a system of charged spots against the neutral background ('hard' version with charged dimples).

Answers to the first two questions are formed even at the initial stage of instability development. As shown in Refs [18, 19], one- or two-dimensional perturbation $\xi(r, t)$ of the surface shape contains different exponents of this amplitude in the nonlinear part of the energy responsible for the appearance of charge continuity breaks, viz. $\xi^4(r, t)$ in one-, and $\xi^3(r, t)$ in two-dimensional case. The two-dimensional scenario appears to be more efficacious since it generates a network of 'bald' spots that eventually develops into a honeycomb corrugation structure [see comments on formulas (2.39)–(2.43)]. An advantage of honeycomb corrugation over other possible two-dimensional lattices is proved by correlation calculations [51] under conditions in which the charged corrugation nuclei are identical and the difference between energies is due to lattice crystallography alone.

The issue of the relationship on average between charged ($s$) and neutral ($1 - s$) fractions of corrugation in the one-dimensional scenario posed in papers [23–25] is unessential because any deep corrugation violates the equipotentiality of the charged boundary in the direction perpendicular to the grooves. Nevertheless, the smallness of $s$ ($s \ll 1$) used in manipulations with functional (2.55) naturally needs to be confirmed [and was — see formula (2.61)] in a series of final results.

The $s$-problem becomes more critical in moving to honeycomb corrugation because, in the case of $1 - s \ll 1$ considered in Refs [23–25], the problem on the whole remains equipotential and its solution is feasible only for $v \ll 1$. The requirement $v \ll 1$ is unessential for describing corrugation by a system of dimples, but it is natural to think that the charged nuclei, with radius $R_s$, of adjacent dimples do not overlap between themselves; in other words, the condition $s \ll 1$ is fulfilled or, in more concrete terms, the condition

$$s \simeq \left(\frac{R_s}{a}\right)^2 \ll 1\,. \tag{2.59}$$

An estimate of $s$ for a honeycomb structure was recently obtained in paper [49] using the cylindrical Wigner–Seitz model under the same conditions as in the one-dimensional scenario [the total dimple charge and the holding field are related to their critical values given by expressions (2.53), (2.54)]. As a result, one finds

$$\frac{R_{\rm crit}}{a} \simeq 0.4 < 1\,, \qquad \frac{\xi_{\rm crit}(0)}{a} \simeq 0.3 < 1\,, \tag{2.60}$$

whence

$$s \simeq \left(\frac{R_s}{a}\right)^2 \simeq 0.16\,, \tag{2.61}$$

suggesting the hard (dimple) reconstruction scenario.

To sum up, reconstruction in the $v \leqslant 1$ region most likely follows the mixed scenario with the energy balance controlled by expression (2.55). Then, variations of groove-like or honeycomb corrugation are feasible in the $\Delta \geqslant 0$ region [$\Delta$ from formula (2.35)]. The mixed scenario predicts no hysteresis phenomena.

It should be noted that the probability of the appearance of multielectron dimples in the $\Delta > 0$ region began to be discussed (see papers [44, 45]) almost simultaneously with the development of the theory of equipotential reconstruction [18, 23]. However, the understanding of the real place of these 'polaron' structures in the hierarchy of states determining the corrugation of a charged helium surface has come only recently [42, 49]. In this sense, the limit $\Delta > 0$, $v \ll 1$ is especially meaningful.

Also of interest in the chronological chain is Ref. [52], in which the scenario of dimple-like reconstruction in the $v \leqslant 1$ region was discussed for the first time. Here, the tight binding approximation provides a basis for theoretical consideration of the problem. The roughly counted free multielectron dimples were regarded as initial ones. Assuming subsequently these quasiparticles to be point-like, the authors of Ref. [52] simulated a periodic lattice of charged dimples using results for a classical Coulomb crystal of point charges [51]. The period of this lattice is determined by a length on the order of the capillary length. Its energy-related advantage over the energies of continuous charge distribution in the 2D layer is interpreted in correlation terms [51].

It should be noted as regards the results of Ref. [52] that the free dimple problem exactly solved in Refs [24, 25] leads under the conditions of work [52] to a charged spot radius much greater than the lattice period from paper [52] (according to Refs [24, 25], in this region $R/a \simeq 1.5$). The critical conditions for dimple formation exceed the dynamic stability threshold. Finally, correlation effects [51] are not directly related to the Coulomb part of the reconstruction problem. Therefore, the approach employed in paper [52] needs to be modified, which was accomplished later by the authors of Ref. [49].

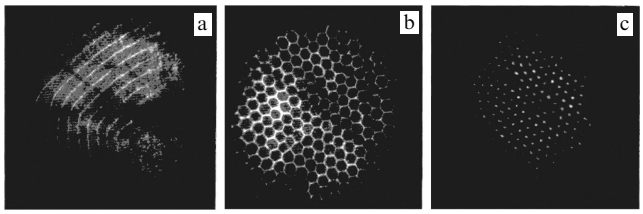


**Figure 9.** Reconstruction of a charged helium surface under conditions of maximum population, $v \leqslant 1$: (a) signs of groove-like reconstruction reproducing the perimeter geometry at small supercriticality values; (b, c) snapshots illustrating reconstruction at finite supercriticality differ in focusing interfering light beams on corrugation ridges and grooves (taken from Ref. [28]).

**2.4.3 The general picture of reconstruction of a charged helium surface.** Let us discuss the current view of the general picture of charged helium surface reconstruction in light of the information presented in the preceding paragraphs and available experimental data. The existence of such reconstruction under the conditions of conservation of the total number of charges on a liquid surface at different occupation levels has been documented in a series of studies [21, 22, 26–28]. Different authors agree that honeycomb corrugation develops in a threshold manner in the region of positive supercriticalities, $\Delta \geqslant 0$. There is no experimental evidence of honeycomb reconstruction in the $\Delta < 0$ region, whereas the region with $\Delta > 0$ and $v \leqslant 1$ exhibits well-defined close-packed corrugation covering the entire charged mirror of the dimple (Fig. 9 [28], Fig. 10 [26, 27]). The dimple depth proves to be finite immediately and grows monotonically with increasing $\Delta > 0$ (Fig. 11 [28]). Where $v \leqslant 1$, the alternative equipotential theory [18, 24, 25] does not work at all, since it

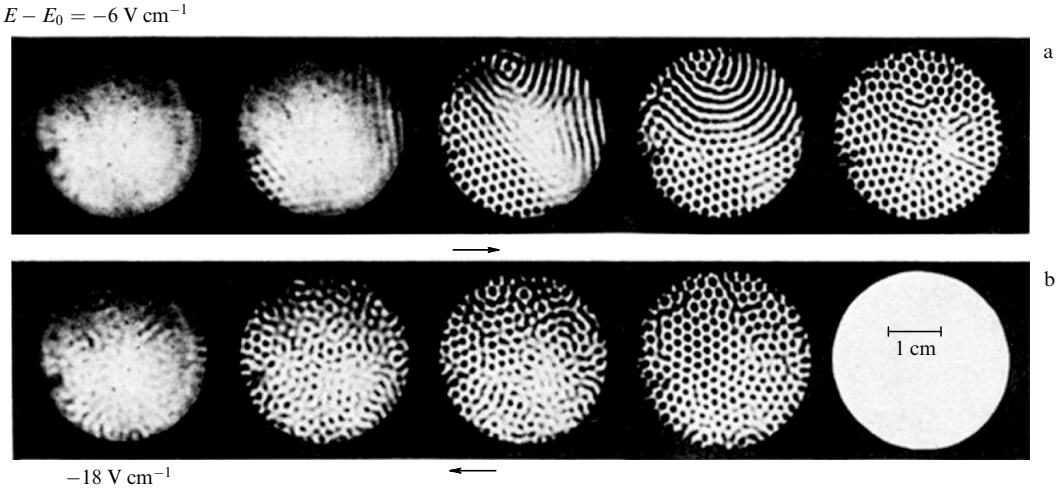


**Figure 10.** Picture of corrugated structure at gradually increasing (a) and decreasing (b) supercriticality $E/E_0$ under conditions of maximum population of the helium surface with electrons [26, 27]. Supercriticality changes stepwise by $\Delta E/E_0$, with $\Delta E = E - E_0 \approx 6$ V cm$^{-1}$. At the initial stages (a), parts of groove-like reconstruction can be seen. The authors of Refs [26, 27] explain it by possible nonhorizontality of the dimples. On the whole, the final state of reconstruction looks glass-like. It is turned into a qualitative honeycomb structure (see Fig. 6) by weak 'annealing' in an alternating electric field. Note also the signs of 'overcooling' in the far left photo in Fig. 6, presumably associated with corrugation establishment kinetics (as in Fig. 6).

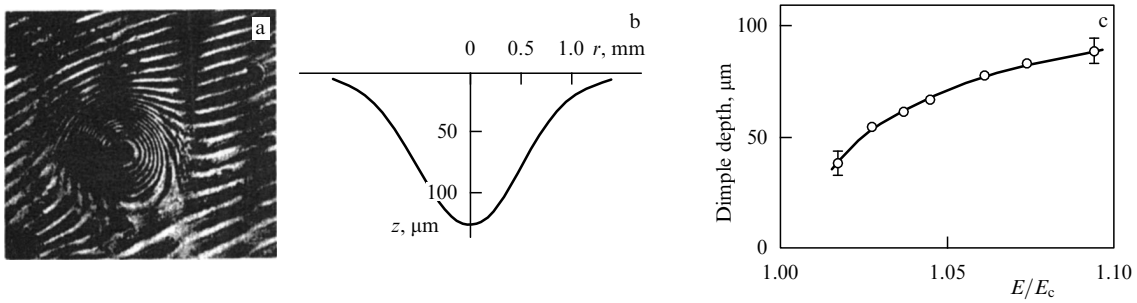


**Figure 11.** (a) Isolated dimple, the profile of which was obtained using the interference technique. (b) Reconstructed profile. (c) Variation of dimple depth depending on the holding field [28].

lacks the smallness of the ratio of the corrugation amplitude to the capillary length (the basic small parameter of the equipotential reconstruction theory). As for the mixed scenario [49], it is intended to explain the phenomena being observed.

As noted above, experimental results for the region with $\Delta > 0$ and $v \ll 1$ do not qualitatively agree with the predictions of the equipotential theory. The observed reconstruction is aperiodic. The helium surface is not subject to periodic corrugation filling the entire liquid mirror, as was expected in Refs [18, 24, 25]. Instead, electrons are grouped into one or more multielectron dimples occupying only a small part of the total helium surface. Figure 7, borrowed from Ref. [28], illustrates a dimple-like reconstruction in the $v \ll 1$ region with gradually increasing $v$. Evidently, the dimple corrugation scenario is energetically preferable (see also Fig. 11), as confirmed in experiment.

A few more words are in order about grooved corrugation observed experimentally at the initial stage of instability development [21, 22, 26–28]. As noted above, groove-like corrugation is on the whole less energetically advantageous than the honeycomb variety. However, near the borders of the charged mirror (or due to dimple nonhorizontality), the corrugation must be conjugated with the local deformation conditions along the boundary of a 2D system. Theoretically, this problem remains unresolved, while experiment gives evidence that grooves actually form along the boundaries (see Figs 9a and 10).

The data presented in the preceding sections suggest an analogy between the reconstruction process and details of the first-order phase transition (binodal-spinodal alternative). The most reliable indicators of such an analogy are the duality in determining conditions promoting the development of reconstruction [see formulas (2.16)–(2.19), (2.32)–(2.34)] and the possibility of drawing a phase diagram separating stability and instability regions of the charged liquid surface in natural coordinates. The following variables appear acceptable: the average population of a helium surface with electrons [$v$ from formula (2.16)] and $\varepsilon_-$, the dimensionless [related to the critical field (2.14)] electric field (2.16) above the charged helium surface. Figure 3 shows a spinodal line, convenient for orientation, which was plotted in these coordinates with the use of 'electrostatic' approximation (2.17). However, the corrections (2.21)–(2.24) indicate that the spinodal cannot approach the axis of ordinates $v \to 0$ with a finite tilt, in contrast to the binodal (2.48), (2.49) calculated with account of phase equilibrium rules. The resulting relative position of the binodal and the spinodal in the region of small $v$ factors is shown in the inset to Fig. 3. The analogy with the general properties of first-order phase transitions (see for instance, Ref. [47]) supports this prediction and substantively explains the observed aperiodic development of reconstruction (formation of isolated multielectron dimples).

Consistent discrimination between the dispersive and fluctuational mechanisms of instability development encounters difficulty at finite (especially maximal) populations $v \to 1$. The same is true of the first-order phase diagrams in the regions where binodals and spinodals are tangent to each other. A distinctive feature of the problem with reconstruction consists in the involvement of both mechanisms in its development. Bearing in mind experimental data that unambiguously suggest periodic reconstruction of a charge-saturated liquid surface, it is possible to eliminate the 'binodal–spinodal' ambiguity, taking into account the temporal evolution of FT decay. As mentioned above [see comments on Eqns (2.11)–(2.15), (2.47), and Figs 3, 4, 10), the spinodal scenario of the decay consistently defines the main details of linear oscillation dynamics and the onset of instability development on a charged liquid surface, thus preparing the system to the appearance of periodically arranged neutral spots in the charge distribution. This picture testifies to the end of spinodal and the onset of binodal evolution with well-defined initial conditions (the charge of a dimple is known, and all dimples are identical).

The scenario with 'spinodal onset' and 'binodal continuation' of deformation of a charged liquid surface may be called naturally a mixed one. The main known factors related to FT decay in the $v \leqslant 1$ region qualitatively correctly co-exist in the framework of this scenario, viz. periodicity of reconstruction, loss of equipotentiality along the corrugated liquid surface, and the stepwise behavior of corrugation amplitude during formation of the stationary reconstructed state of the liquid boundary.

The verbal description of charged helium surface reconstruction can be supplemented by the data integrated into a graphical phase diagram. Figure 12 represents in the $v-\varepsilon_-$ coordinates such a combination of the plots from Fig. 3 and the experimental information on reconstruction in different limits in $v$. Here, $v$ is defined by formula (2.16), and $\varepsilon_-$ is a dimensionless electric field [related to the critical one (2.14)] above the charged helium surface. The solid curve describes the behavior of the critical $v$ value as a function of voltage $\varepsilon_-$ starting from zero for the dynamic instability scenario (spinodal, in the phase language). As shown before, the reconstruction in the $v \leqslant 1$ region follows a mixed scenario. It becomes aperiodic for $v \ll 1$, taking on the appearance of individual solitons interacting among themselves. The photographs-insets illustrate the real shape of the corrugated

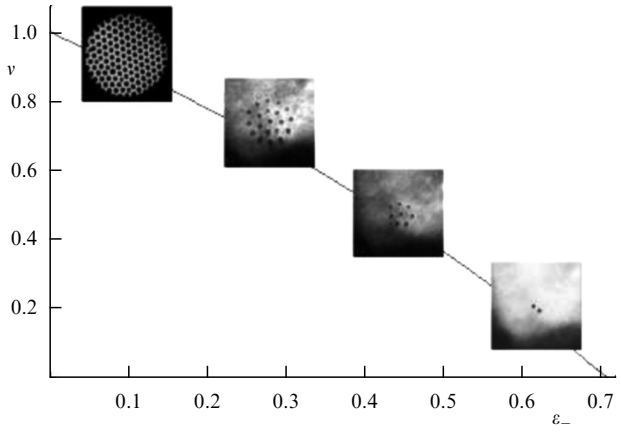


**Figure 12.** Phase diagram [49] of the reconstruction process at the helium liquid–vapor interface in the presence of a fixed charge with different degrees of occupation, $\nu$, depending on the reduced electric field $\varepsilon_-$ above the helium surface. The snapshots-insets illustrate the state of the helium surface at a given degree of occupation. The top left part of the diagram corresponds to the quasispinodal scenario of corrugation appearance. The bottom right part is typically binodal.

surface. The bottom right one correlates with Fig. 3 and corresponds to the binodal plane–single dimple transition. The two central photos correspond to a certain intermediate state in the presence of dimple–dimple interaction [see formula (2.51)]. The close-packed picture shown in the top photo corresponds to an intermediate scenario of decay with the spinodal onset (see Fig. 3) and binodal end. The continuity of filling an increasingly larger area of the liquid surface with the dimples is implied (but not proved).

## 3. The charged thin liquid film

### 3.1 Introductory notes

A metallic substrate is one of the important factors influencing the character of instability and details of corrugation formation on a charged liquid surface. The effect of a substrate growing with monotonically decreasing thickness $d$ of a liquid film in the region of $\tilde{\kappa}d < 1$ ($\tilde{\kappa}$ is the effective capillary constant of the film problem depending on the details of its setting up) accounts for the film reconstruction problem being a self-consistent problem requiring special consideration. The changes are purely formal (the Coulomb part of the problem simplifies, and the boundary condition problem arises); modification of the dispersion law results in a more diversified picture of deformation phenomena, and, finally, in hydrogen films (a mere detail) variations in the reconstruction are feasible, both with a fixed total charge and with a given external potential.

In analogy with the 'bulk' problem, we shall start considering 'film' results from the discussion of the stability problem for an infinitely extended film. Edge effects can be neglected here if the main events occur at wavelengths that are small compared with the film dimensions along the substrate. An additional simplification (also arising from the 'bulk' problem) concerns conductivity of a film surface regarded as ideally conducting. An advantage of the 'unconstrained' approach is uniformity of the linear description of the instant of stability loss in a charged film allowing for a consistent interpretation of the limits of bulk ($\tilde{\kappa}d > 1$) and film ($\tilde{\kappa}d < 1$) problems. The boundedness manifests itself as the impossibility of considering edge effects that are much more diverse in the charged film problem than in the bulk case. In particular, an inhomogeneous variant of stability loss absent in the bulk problem acquires significance. Formally, the question at issue is an inhomogeneous system of equations, and, therefore, deformation of a charged liquid surface develops in a thresholdless manner after the appearance of finite charge density on it. The effect of thresholdless deformation is present in the bulk problem, too [see formulas (2.4)–(2.8)], where deformations of these two types seem to be independent. In the film, however, the thresholdless solution ceases to be stable as the destabilizing field increases. Parametrically, the threshold looks like that in an infinite problem (although it is not evident in advance). But the numerical coefficient is highly sensitive to the boundary conditions at the film edges.

The development of events in the region of parameters exceeding the critical ones, including the reconstruction problem, is discussed in Section 3.2. Here, the restoration of the alternative is of qualitative interest; namely, the stationary reconstruction of a charged film becomes possible not only under conditions of conservation of the total number of charges on it but also when a fixed value of electric potential is maintained along the film. As a matter of fact, the film problem differs from the bulk case in that the latter contains no proof of the impossibility of such a course of events for technical reasons (the lack of a regular perturbation theory) and direct experiments remain to be performed, while the former exhibits both opportunities.

### 3.2 Instability of a charged thin liquid film

A. It is natural to begin discussing this issue from the stability problem as in the case of a charged liquid surface (see Section 2). The set of equations (2.10) with the boundary conditions for potentials $\varphi$ and $\Phi$ at finite $d$ and $h$ (Fig. 1a) gives the following expression for the spectrum of small oscillations, derived for the first time by Chernikova [53]:

$$\omega^2 = \frac{k\tanh(kd)}{\rho}\left\{\rho g + \alpha k^2 - \frac{k}{4\pi}\left[E_-^2\coth\left(k(h-d)\right) + E_+^2\coth(kd)\right]\right\}. \qquad (3.1)$$

The general dependence (3.1) simplifies in the cases of symmetric ($h - d = d$) and asymmetric ($h \to \infty$) geometry.

In the former case, according to formula (3.1), one obtains

$$\omega^2 = \frac{k\tanh(kd)}{\rho}\left[\rho g + \alpha k^2 - \frac{k}{4\pi}\left(E_-^2 + E_+^2\right)\coth(kd)\right]. \qquad (3.2)$$

Formally, the parameters of the problem corresponding to the stability boundary are defined by simultaneous solution of equations

$$\omega(k) = 0\,, \qquad \frac{\partial\omega^2}{\partial k} = 0\,. \qquad (3.3)$$

The analysis of conditions (3.3) that requires the application of numerical methods in the transition region leads in the symmetric limit to the results presented in Fig. 13 [53]. Curve *1* depicts a variation of $E_{+c}^2 + E_{-c}^2$ depending on $d/a$, and curve *2* illustrates the behavior of $k_c a$ as a function of $d/a$.

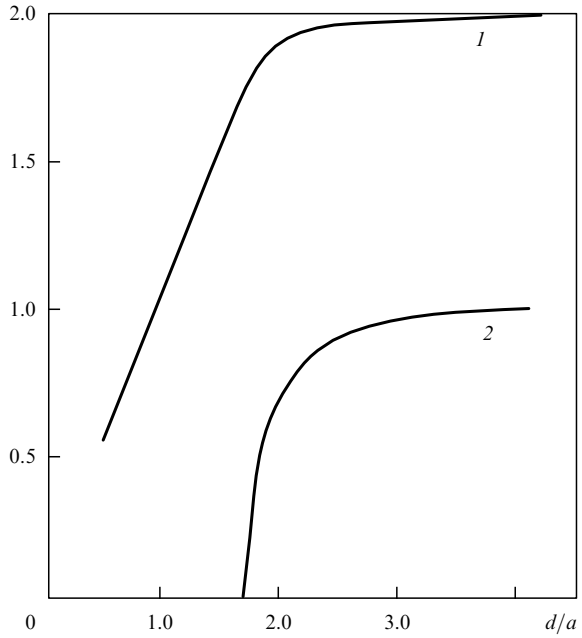


**Figure 13.** Properties of a charged thin film: curve *1* — dependence of the critical field in a film on its thickness $d/a$ in capillary lengths, referred (for convenience) to half of the critical field in the case of charged semispace; curve *2* — dependence of the critical wave number of a film on its thickness $d/a$, referred to its critical value for the charged space [53].

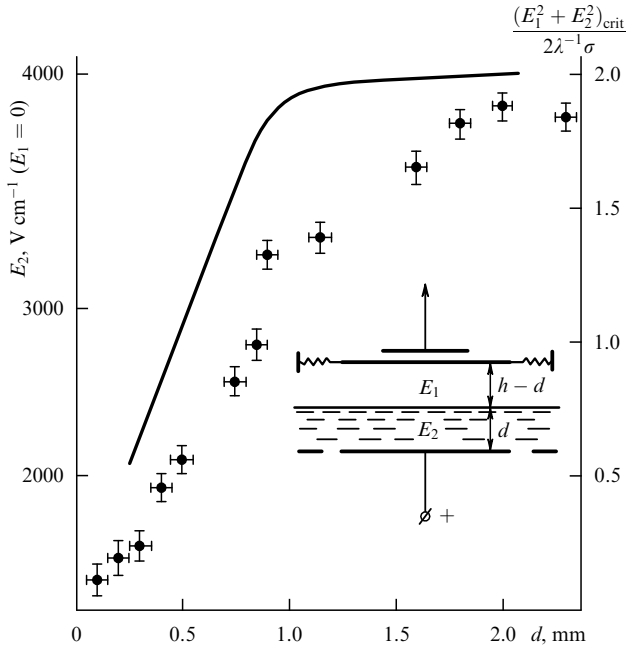


**Figure 14.** Experimentally found film-thickness dependence of the critical field of a charged helium film at a constant total charge on its surface [40]. Solid curve — theoretical prediction [53]. Inset — schematic of the experimental setup [40].

The most interesting corollaries of formulas (3.3) and the results presented in Fig. 13 include the vanishing of the critical wave number $k_c$. Near the threshold $d_0$, one has

$$k_c^2 = \frac{d^2 - d_0^2}{a^2 d^2}, \qquad d_0 = \sqrt{3}\, a. \tag{3.4}$$

In the region $d/d_0 < 1$, the critical electric field also appreciably diminishes:

$$E_{+c}^2 + E_{-c}^2 \simeq 4\pi\rho g d. \tag{3.5}$$

Accordingly, the critical electron surface density is given by

$$n_s^{cr} \simeq \frac{1}{e}\sqrt{\frac{\rho g d}{4\pi}}. \tag{3.6}$$

Analysis of the asymmetric case does not change the qualitative conclusions (3.4)–(3.6). Instability moves into the region of small wave numbers, and critical parameters 'drop' until van der Waals forces come into play.

Notice also that all experiments with helium films were carried out at $E_- = 0$ without regard to any special considerations, besides a relatively simple possibility of estimating charge density. For this reason, the problem of infinite film stability at arbitrary occupation $\nu$ and its role in the formation of corrugation variants (considered in Section 2 for a charged liquid surface) is not discussed below.

The results of Ref. [40] deserve special mention among the experimental findings obtained in this field; they illustrate the initial stage of $\kappa d$-dependence of critical characteristics of the charged helium film in the $\kappa d \leqslant 1$ region (Fig. 14).

B. There are two generalizations of the picture reported in paper [53]. First, the notion of gravity in the stability problem undergoes modification with film thinning. Van der Waals forces come into play, which radically changes the results obtained. Second, it is interesting to observe the behavior of the stability problem when the substrate is other than metallic and has finite permittivity. Relevant corrections [54] lead to the dispersion law

$$\omega^2 = k\left[\left(\frac{3f}{\rho d^4} + g\right) + \frac{\alpha}{\rho}k^2 - \frac{4\pi e^2 n^2}{\rho}\, k\, \frac{1+\delta\exp(-2kd)}{1-\delta\exp(-2kd)}\right]\tanh(kd). \tag{3.7}$$

Here, $f$ is the van der Waals constant, $\delta = (\epsilon - 1)/(\epsilon + 1)$, and $\epsilon$ is the permittivity of the substrate ($\epsilon = \infty$ for a metal). The van der Waals forces are represented here by an unretarded variant, $d < d_W$, where $d_W$ is the characteristic van der Waals thickness. In the general case, van der Waals pressure is defined as

$$P_W(\zeta) = \frac{f}{d^3}\left(1 + \frac{d}{d_W}\right)^{-1}. \tag{3.8}$$

Interpolation formula (3.8) taking account of the retardation effect was proposed in Refs [55, 56]. The measurement of $f$ and $d_W$ constants entering formula (3.8) is a special problem. In the case of superfluid helium, the values of these constants ensue from the analysis of third-sound propagation [56]. Clearly, law (3.7) can aspire to quantitative assertions only in the $d \leqslant d_W$ region, which is the point of interest here though.

The solution of the system of equations (3.3) taking account of law (3.7) yields the critical value of surface charge density $n_s^{cr}$ and the respective critical value of wave vector $k^{cr}$ as a function of $d$. The asymptotic behavior of these quantities

in thick films for $k^{\rm cr}d \gg 1$ ($d > 10^7$ Å) is independent of substrate permittivity:

$$n_{\rm s}^{\rm cr} = \left[\frac{\alpha}{4\pi^2 e^4}\left(\frac{3f}{d^4} + \rho g\right)\right]^{1/4}, \qquad (3.9)$$

$$k^{\rm cr} = \frac{2\pi e^2 (n^*)^2}{\alpha}. \qquad (3.10)$$

For thin films ($d < 10^3$ Å) deposited on a metallic substrate, the following asymptotic expression was obtained taking account of $kd \ll 1$:

$$n_{\rm s}^{\rm cr} = \left(\frac{3f}{4\pi e^2}\right)^{1/2} d^{-3/2}. \qquad (3.11)$$

This means that taking account of van der Waals forces alters the character of the film-thickness dependence of critical charge density: the value of $n_{\rm s}^{\rm cr}$ passes through a minimum as $d$ monotonically decreases, and sharply increases thereafter.

The general picture of $n_{\rm s}^{\rm cr}(d)$ and $k^{\rm cr}(d)$ behavior is presented in Fig. 15.

C. An additional beautiful detail emerges when deformation $\bar{d}$ is taken into account in the problem of critical parameters in the region of action of van der Waals forces. These forces lead to renormalization of critical parameters of a charged film [see formulas (3.9)–(3.11)]. Moreover, they play an important role in the formation of the film. In the present case, the analog of the problem (2.5)–(2.8) is the calculation of the van der Waals film thickness in the presence of fixed charge density $n_{\rm s}$ at the film surface. The result from paper [57] is as follows:

$$d_{\rm W}^{-1} = \left(\frac{1}{d_0^3} + \frac{2\pi e^2 n_{\rm s}^2}{f}\right)^{1/3}, \qquad d_0 = \left(\frac{f}{\rho g h_0}\right)^{1/3}, \qquad (3.12)$$

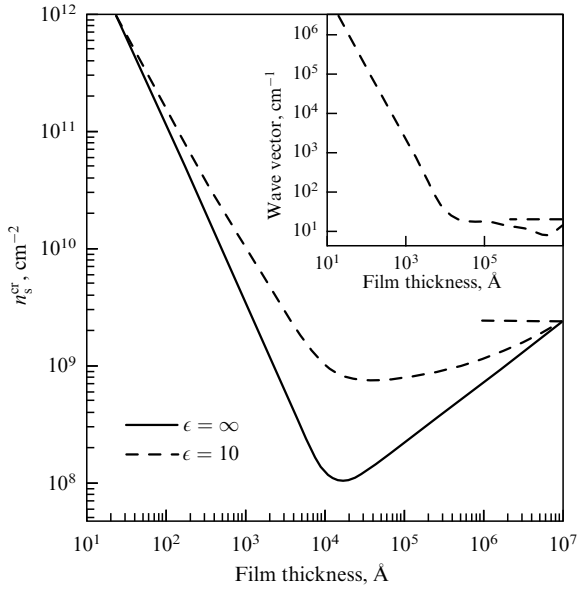


**Figure 15.** Film-thickness dependence of critical charge density and critical wave vector (inset) according to dispersion relation (3.7) in the presence of a metallic (solid curve) or dielectric (dashed curve) substrate at $\epsilon \approx 10$, and $f \approx 9.5 \times 10^{-22}$ J [54].

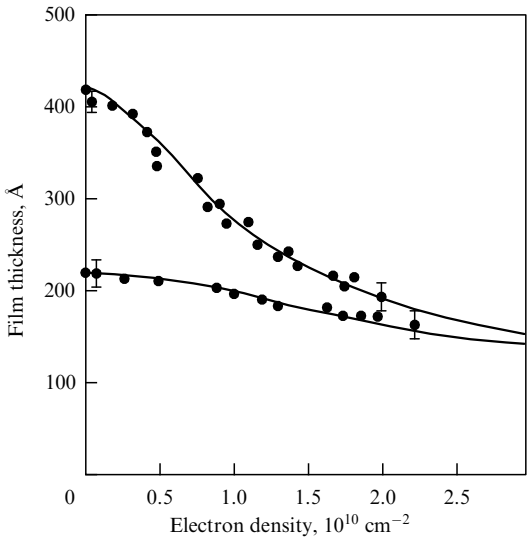


**Figure 16.** Effective helium film thickness plotted vs electron density. Curves — results of calculations by formula (3.12) for two neutral films of initially different thicknesses. Circles — experiment [57] with varied electron density at the film surfaces. The difference among film thicknesses gradually decreases with increasing electron density, as predicted by the theory (see paper [58] and Fig. 17).

where $h_0$ is the height of the solid substrate above the liquid helium level, and the holding electric field strength has the maximum value $E_\perp = 2\pi e n_{\rm s}$.

The experiment reported in paper [57] confirms the substantial relation between $d$, $f$, and $n_{\rm s}$. According to Eqn (3.12) (solid curves in Fig. 16), electron pressure may cause a severalfold change in the film thickness.

Turning back to the discussion of the critical parameters of the charged film, one has to obviously correlate two processes, viz. the growth in the critical $n_{\rm s}^{\rm cr}$ value with decreasing $d$, and the reduction in $d$ with increasing the level of film charging. The co-existence of these two trends is illustrated in Fig. 17 [58]. Curve *1* is analogous to the dependence $n_{\rm s}^{\rm cr}(d)$ in Fig. 15 for $\epsilon \to \infty$ and unretarded van der Waals forces. Curves *2–5* reflect the process of film thinning with increasing charge density (for films of different initial thicknesses). The real critical density for a film of thickness $d_0$ is given by the intersection of curves *1* and *2–5*. Evidently, the critical density is increasingly less dependent on $d_0$ as the last quantity decreases; formally, it tends toward infinity.

The traces of the influence of film thickness deformation on $n_{\rm s}^{\rm cr}(d)$ can be seen right of the minimum of curve *1* (see Fig. 17). Curve *2*, starting from a certain $d_0$ value of the neutral film, meets, due to its deformation, the general dependence $n_{\rm s}^{\rm cr}(d)$ at point $d < d_0$ under the effect of electron pressure; this effectively corresponds to a fall in the critical surface density compared with the calculated one [57]. The final results of such correction of $n_{\rm s}^{\rm cr}(d)$ taken from Ref. [59] (that proved to be useful) are shown in Fig. 18, together with the theoretical result presented earlier in Fig. 14, data obtained in Ref. [40] (light circles) and those, as reported by a French group (dark circles), covering the interval $\kappa d \leqslant 1$ somewhat greater than in Ref. [40] and extended toward the reduction of this parameter.

D. The qualitative difference between the surface and film stability problems also holds for the conditions of conserva-

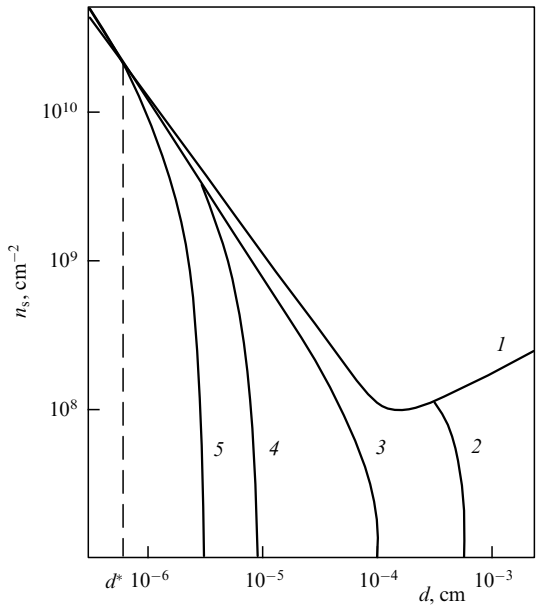


**Figure 17.** Variation of critical electron density depending on the effective helium film thickness (curve *1*) with a decrease in the initially different film thicknesses under the effect of growing electron pressure (curves *2–5*) (taken from Ref. [58]).

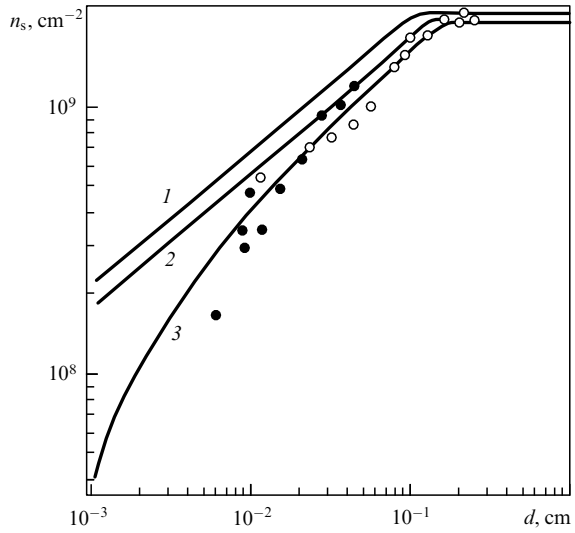


**Figure 18.** Correction of theoretical prediction [53] taking account of helium film deformation under the effect of electron pressure [59]. Curve *1* — the plot borrowed from Ref. [53] (see Fig. 14 for details); curve *2* — calculated corrections for deformation at $E_- = 0$; curve *3* — critical charge density at the helium film surface taking account of corrections for deformation at $E_- = 300$ V cm$^{-1}$ [59]; light circles — measured values [40], dark circles — data from Ref. [60].

tion of the electric potential $V$ (rather than the total charge or its density) on a charged surface. The primary cause of such difference lies in electrostatic definitions. Given the geometry of the structure shown in Fig. 1, it is easy to see [assuming complete field shielding above the film ($E_- = 0$) and using information on the long-wavelength character of the film instability development] that in the case of fixation of the total charge (hence, charge density along film edges), the main part of stress tensor $E_+^2/8\pi$ appearing in pressure balance on the film surface is unrelated to its thickness $d$ and, therefore, can be neglected as in the bulk case. However, the maintenance of $V$ changes the picture. Characteristic electric fields

$$E_+ = \frac{V}{d}\,,$$

and, therefore, the stress tensor $E_+^2/8\pi$, begin to 'adhere' to variations in the position of the free film surface if $\xi/d \leqslant 1$, where $\xi(x, t)$ is the film surface oscillation amplitude. There is no such adhering in the bulk case where $\xi/d \ll 1$. This means that all nonlinear phenomena on the helium film in the problem with $V = \text{const}$ need to be reconsidered.

In so doing, the first issue is the equilibrium properties of a helium film in a plane capacitor (see Fig. 1) with potential $V$ across its plates under conditions of $E_- = 0$. The consideration is analogous to that in Section 2 [see formulas (2.4)–(2.8)] with the substitution of

$$\frac{V}{d} \to \frac{V}{d + \xi_0}\,.$$

As is shown in Ref. [61], the solution of this inhomogeneous one-dimensional problem leads to film deformation $\xi_0$ in the form

$$\xi_0 \sim \frac{V^2}{(d + \xi_0)^2}\,. \tag{3.13}$$

The behavior of deformation $\xi_0$ is apparent in the region of small $V$. Here, $\xi_0$ increases in a thresholdless manner at the initial stage of capacitor voltage growth (Fig. 19). However, a rise in $V$ results in appearance of a threshold $V_c$:

$$V_c^2 = \left(\frac{2}{3}\right)^3 V_0^2\,\frac{g^*}{g}\,, \qquad V_0^2 = 4\pi\rho g d^3\,, \tag{3.14}$$

$$g^* = g\left(1 + \frac{L}{L_0 - L}\right) \tag{3.15}$$

($L$ and $L_0$ are marked in Fig. 1), bringing about the loss of stability. Here, $V_0$ is the threshold voltage (3.5) from the 'infinite' film stability problem, and $\xi_0$ at the critical point ($\xi_0 = \xi_0^{\text{crit}}$), namely

$$\xi_0^{\text{crit}} = -\frac{d}{3}\,,$$

is comparable to the initial film thickness.

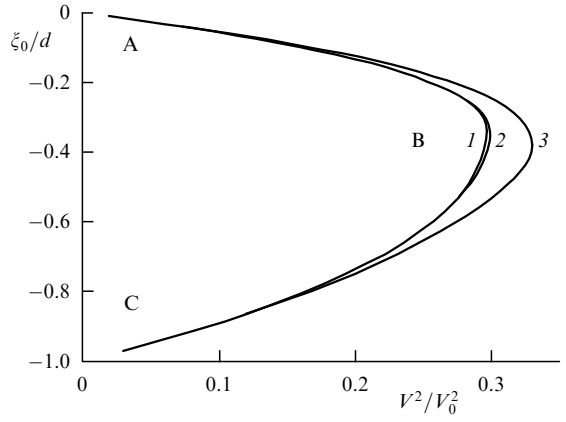


**Figure 19.** The behavior of helium film deformation $\xi_0(v^2)$ under equipotentiality conditions for different lateral dimensions $\kappa L$: curve *1* — $\kappa L = 10$; curve *2* — $\kappa L = 2.5$, and curve *3* — $\kappa L = 3.1$ [62]. AB — stable, and BC — unstable portions ($v^2 = V^2/V_0^2$).

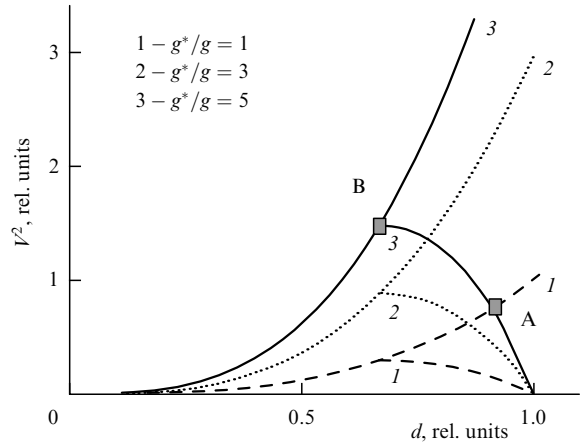


**Figure 20.** Diagram showing the critical field strength for a helium film undergoing deformation.

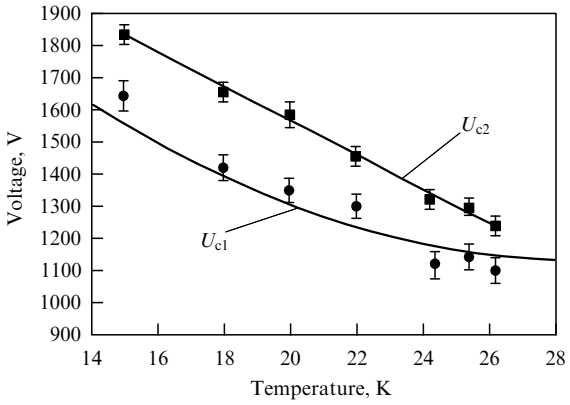


**Figure 21.** Experimental temperature dependence of critical voltage $U_{c1}$ [63]. The curve shows results of calculations in accordance with Ref. [53]. Note a better correspondence between calculated and observed data than in Fig. 14, one of the possible causes being manifestation of an alternative mechanism (3.14) of instability development. Also presented are the respective characteristics of the upper critical field $U_{c2}$.

The picture of what is happening is supplemented by the interaction of two factors, viz. the thickness dependence of liquid film field stability and the change in film thickness under the action of electron pressure (effects analogous to those in Figs 16, 17). Taken together, these factors in the region to the left of the minimum in the diagram in Fig. 15 are responsible for the absence of the instability effect. Interpretation of these phenomena to the right of the minimum needs modification if $g^* \neq g$.

The diagram in Fig. 20 gives the critical field strength for a helium film subject to inhomogeneous electron deformation at different $g^*$. The pairs of curves *1–1*, *2–2*, and *3–3* correspond to $g^*/g = 1, 3, 5$, respectively. The curves issuing from a point $d = 1$ show how deformation of a charged surface increases in the cell center with growing voltage. The respective curves reflecting the dependence $(3/2)^3 V_c^2 = 4\pi\rho d^3 g^*/g$ demonstrate the behavior of the critical voltage following alteration of the film thickness. The intersection point of the curves with similar indices corresponds to the loss of stability caused by liquid deformation. At $g \sim g^*$, the critical voltage $V_c$ turns out to be lower than $V_0$, in accordance with formula (3.14). On the other hand, the larger $g^*$, the higher the critical voltage. The position of point A (see Fig. 20) below B means that the critical deformation voltage of a finite film is higher than the critical voltage corresponding to the loss of stability of an infinite film.

The method realized in experiments with a charged hydrogen antifilm [63] makes it possible to identify the mechanism of instability (3.14) alternative to that described by formula (3.5) (see Figs 19 and 20). The authors used a closed container with a liquid condensed from the inflowing gas. The lateral diameter of the cell was roughly 1.2 cm. The vacuum gap between the upper electrode and the condensed liquid surface played the role of the antifilm. Under isothermal conditions, manipulations with the liquid component of such a system were difficult to control. But the level of the liquid in the container could be established at any desired height by varying the amount of the gas in the cell and the temperature difference produced when the bottom of the vessel was mildly cooled with respect to the ambient temperature.

By charging a liquid hydrogen surface with ions from the inside [the only way to charge the surface when the gap between the liquid and the upper electrode (antifilm) is sufficiently small] and keeping the cell saturated in the course of the experiment (with the liquid surface being equipotential), it is possible to make the liquid surface lose stability (by varying the vacuum gap thickness), to form a soliton state in supracritical conditions, and, finally, to cause a breakdown of the charged boundary (by further increasing the degree of supercriticality) as proposed in Ref. [53] or in accordance with the scenario illustrated in Fig. 19. The critical conditions from Ref. [63] are represented in Fig. 21 where the abscissa is the temperature (instead of the film thickness $d$) unambiguously determining the value of $d$. The experimental data reported in paper [63] fairly well reproduce Chernikova's predictions [53]. The same figure contains information about the upper critical field.

When discussing the degree of correlation between the experimental data from Ref. [63] (see Fig. 21) and Ref. [40] (see Fig. 14) and the theory [53], it is unfortunately worth noting the absence of details of these measurements important for the interpretation of the available alternative (different conditions of filling the film surface with electrons, and incomplete information about cell geometry preventing estimation of the difference between $g_*$ and $g$). What is certain are the real physical causes suggesting the possibility of different origins of instabilities in the cases illustrated in Figs 21 and 14. The authors of Ref. [63] did not try to decide between two alternatives (either [53] or [61]) and, therefore, did not use the obvious way to come to a conclusion, i.e., variation of the parameter $g^*/g$. A better agreement between theory [53] and experiment [63] than in Ref. [40] may be due to the variativity of definition (3.14). The equipotential scenario of instability development is especially noticeable at the final stage of soliton formation during reconstruction (see Section 3.3).

E. To sum up the foregoing, let us briefly outline the current state of the 'film' problem. The most distinctive feature in the behavior of the system of electrons above a helium film is the nonmonotonic dependence of the critical parameters of 2D electrons on the film thickness. This fact was partly documented by independent data [40] (see Fig. 14) to the right of the minimum of function $n_s^{cr}(d)$ and, accordingly, by

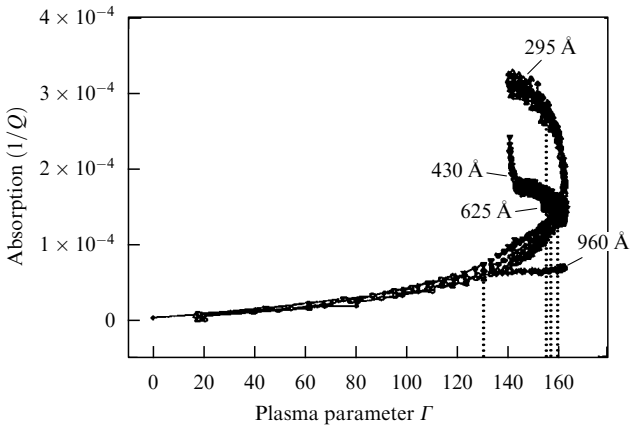


**Figure 22.** Absorption (or inverse quality factor $Q^{-1}$ of the resonator) of the high-frequency energy by electrons on a helium film of variable thickness, which were placed at the electric field antinode of the resonator. Plasma parameter $\Gamma = V_C/T$, where $V_C$ is the mean Coulomb energy of electrons in the 2D system, increases with a rise in the critical electron density caused by the film thinning (the phenomenon left of the minimum of curve *1* in Fig. 17). The growth in $\Gamma$ is accompanied by monotonic increase in absorption until this parameter reaches the critical value $\Gamma \leqslant 160$. The nonmonotone behavior of $Q^{-1}$ observed in this region is interpreted as the arrival of the 2D system in the Coulomb crystallization region and its transition to a state with quantum melting of the electron Coulomb crystal [64].

measurements [57] (see Fig. 16) on the left shoulder of this extremum. Measurements in the region of the minimum itself have not yet been made. The real thickness of the film needs to be corrected practically within the entire range of $\kappa d \leqslant 1$ in view of the action of electron pressure on it. This effect is especially noticeable left of the minimum of $n_s^{cr}(d)$ (see Fig. 16). On the right-hand side of the $n_s^{cr}(d)$ diagram, the correction must take into account variations of the film thickness under the action of electron pressure pursuant to the scheme illustrated in detail in Fig. 20.

An interesting possibility of increasing critical electron density at the left shoulder of the $n_s^{cr}(d)$ diagram (up to the appearance of signs of degeneration in the 2D system) stimulated serious efforts [64] to reveal this effect, which is of importance from the standpoint of overlapping conditions for the existence of classical and degenerate 2D ensembles and determining the upper melting limit of the Coulomb crystal. Figure 22 [64] illustrates the position of the transition region at the plane: absorption as a function of plasma parameter $\Gamma$ of the problem for an electron Coulomb crystal on a helium film, and parameter $\Gamma = V_C/T$, where $V_C$ is the mean Coulomb energy of electrons in the 2D system, and $T$ is the temperature.

### 3.3 Charged solitons on a thin helium film

A consistent picture of transition from the flat to the corrugated state for the 'bulk' problem is to a large extent based on the qualitatively acceptable mechanism of charge distribution between the emerging dimples (each dimple traps electrons in a region with a radius on the order of capillary length). Such heuristic arguments are absent for a charged film with instability in the vicinity of small wave numbers. For this reason, the section concerning dimples and other soliton structures on a liquid film can be formulated only as a description of separate episodes without pretension to building (as in Section 2 above) a general phase diagram of the flat state transformation to the corrugated one. Part of the present section is devoted to a discussion of alteration in the properties of multicharged dimples with gradual film thinning. In what follows, we consider the most interesting possibility of the formation of qualitatively new charged soliton structures with equipotential electrostatics.

A. *Isolated multicharged film dimples versus thoroughly explored 'bulk' analogs* [65]. Let us consider a multielectron dimple on a helium surface of thickness $d$ underlain by a bulk metallic substrate. The influence of the finite film thickness on dimple parameters touches several parts of the problem. First, the interaction of electrons and the metallic substrate modifies the effective holding field:

$$E = E_\perp + \frac{F_d}{e}, \qquad F_d = \frac{e^2}{4d^2}, \tag{3.16}$$

where $E_\perp$ is the external electric field, and $F_d$ is the image force.

Second, film thickness $d$ appears in the definition of dimple Coulomb energy. Because the Coulomb energy over 'bulk' helium has the form

$$W_C = c_0 \frac{Q^2}{R}, \qquad Q = eN, \qquad c_0 = 15.73 \tag{3.17}$$

($R$ is the radius of the charged spot in the dimple center, and $Q$ is the total dimple charge), it must be expressed at the film under conditions $d/R \leqslant 1$ as

$$W_C = \frac{2dQ^2}{R^2}. \tag{3.18}$$

Interpolation of asymptotics (3.17), (3.18) gives the definition of energy

$$W_C = \frac{c_0 Q^2}{R(1 + c_1 R/d)}, \tag{3.19}$$

where $c_1$ is a constant on the order of unity. Finally, the definition of effective capillary constant $\tilde{\kappa}$ changes:

$$\tilde{\kappa}^2 = \frac{\rho \tilde{g}}{\alpha}, \qquad \tilde{g} = g + \frac{3f}{\rho d^4} \frac{1}{1 + d/d_*}. \tag{3.20}$$

The van der Waals constant $f$ has a scale of $\sim 60$ K, and $d_*$ is the characteristic length arising in the theory of van der Waals forces taking account of retardation effects.

The total energy of a multielectron dimple on a helium film is possible to represent in analogy with the bulk case [44, 45] as

$$W = \frac{Q^2 E_\perp^2}{8\pi\alpha} \exp\left(\frac{\tilde{\kappa}^2 R^2}{2}\right) \mathrm{Ei}\left(-\frac{\tilde{\kappa}^2 R^2}{2}\right) + V_C(Rd), \tag{3.21}$$

where $R$ is the variable parameter, while $N$, $E_\perp$, and $d$ have fixed values.

It is convenient to introduce a dimensionless electric field $\lambda$ and film thickness $\tilde{d}$:

$$E_\perp^2 = \lambda \kappa_0 \alpha, \quad \kappa_0^2 = \frac{\rho g}{\alpha}, \quad \tilde{d} = \frac{d}{d_0}, \quad d_0 = \left(\frac{3f}{\rho g}\right)^{1/4} \approx 10^{-4}\,\mathrm{cm}. \tag{3.22}$$

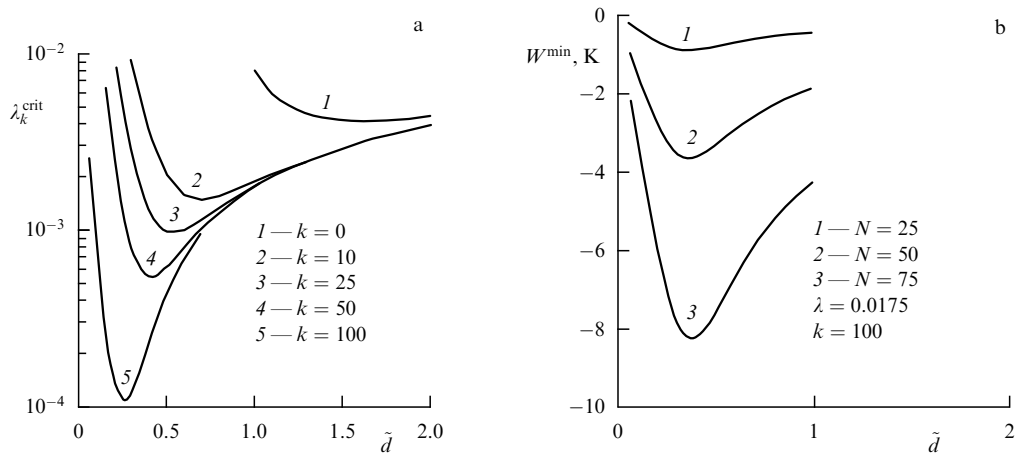


**Figure 23.** (a) Plots of dimensionless critical field $\lambda^{\rm crit}$ versus effective film thickness at different values of parameter $k = \tilde{d}/d_0$. (b) The energy $W^{\rm min}$ of dimples with different numbers of electrons plotted versus the effective film thickness.

The dimple is stable as in the bulk case if

$$W(\lambda_k^{\rm crit}) \approx 0\,. \tag{3.23}$$

The corresponding plot of function $\lambda_k^{\rm crit}(\tilde{d})$ at different values of the parameter $k = d_*/d_0$ is presented in Fig. 23a. It can be seen that parameter $k$ markedly affects the diagram. When $k = 0$, retardation effects are neglected. Figure 23b demonstrates the dependence of the dimple energy $W$ on the dimensionless film thickness at a fixed $\lambda$ value and a different number $N$ of electrons in the dimple. The value of $N$ was optimized by the requirement that the energy had a scale in excess of the experimental temperature close to 1 K. Importantly, the position of the minimum of $W^{\rm min}(\tilde{d})$ is insensitive to $N$, meaning that multielectron dimples differing in $N$ and emerging as the film loses stability have a maximum binding energy at a $\tilde{d}$ value equal for all $N$.

In addition to a series of calculated plots, we display an image [63] of a film dimple with a fixed charge number (Fig. 24). This image may be useful for comparing the dimple profile with equipotential soliton geometry (see Fig. 26 below).

Of importance for the development of reconstruction is not only the appearance of individual multicharged dimples on the liquid surface but also the character of their interaction. A comparison of 'bulk' [see Section 2, formulas (2.50)–(2.52)] and 'film' dimples reveals their qualitative identity. As in the case of interdimple interaction energy (2.50), the film exhibits strain-induced attraction between the dimples stronger than that in the bulk case. In contrast, the electrostatic repulsion is markedly weakened (dipole–dipole instead of Coulomb). As a result, individual dimples emerging in the course of reconstruction must merge into one another.

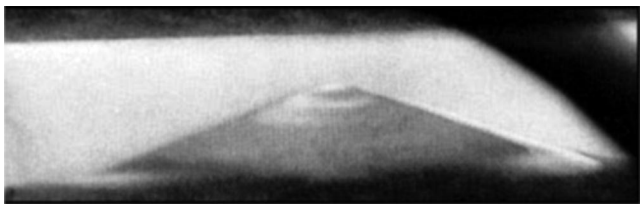

**Figure 24.** Photo of an antifilm dimple with a fixed charge [63]. The lateral dimension of the dimple is roughly 1.2 cm. The capillary length of liquid hydrogen is on the order of 0.19 cm.

B. *A variant with a very pronounced $R/d \gg 1$ ratio*. In this hypothetical regime, one finds

$$W \simeq W_{\rm C} + W_\xi + W_{\rm edge}\,, \tag{3.24}$$

$$W_{\rm C} = \frac{2\pi(d+\xi)Q^2}{S}\,, \quad W_\xi = \alpha\tilde{\kappa}^2\xi^2 S\,, \quad W_{\rm edge} \propto \sqrt{S}\,,$$

$$Q = en_{\rm s}S\,, \quad S = \pi R^2\,,$$

where $W_{\rm C}$ is the Coulomb energy of a flat capacitor, $W_\xi$ is the deformation energy of gravitational origin, $W_{\rm edge}$ is the contribution to the total energy of the boundary origin, and $Q$ is the total charge of a disk having area $S$ at the film surface.

Reducing the energy (3.24) with the omitted contribution of $W_{\rm edge}$ to a minimum in $\xi$ and substituting the result into the initial expression, one arrives at

$$W \simeq 2\pi e^2 n_{\rm s}\left(d - \frac{e^2}{\alpha\tilde{\kappa}^2}\,n_{\rm s}^2\right)N\,, \qquad n_{\rm crit}^2 = \frac{d\alpha\tilde{\kappa}^2}{e^2}\,. \tag{3.25}$$

Evidently, there is no solution with the finite values of $Q$ and $S$ in the present scenario. The system of electrons either occupies the whole available area $S_\infty \gg S$ for $n_{\rm s} < n_{\rm crit}$ or collapses into a point for $n_{\rm s} > n_{\rm crit}$. This conclusion logically continues the analysis described in paragraph A of this section; namely, an isolated dimple with a large enough number of electrons is unstable and cannot exist in the form of a charged disk with radius $R/d > 1$ in the right branch of the plot in Fig. 17. The respective structures 'sink' to the stable left part of this dependence arising from a sharp increase in $\tilde{\kappa}^2$ in the region subject to the action of van der Waals forces. Figure 25 illustrates such behavior of solitons.

C. *Solitons on an equipotentially charged helium film under conditions $V = {\rm const}$*. This case brings us back to the problem of the realization of the equipotential (homogeneous) or inhomogeneous reconstruction scenario raised in the Introduction. For the 'bulk' problem under the conditions of the conservation of a total charge, the equipotential recombination variant proved unrealizable (because of emerging

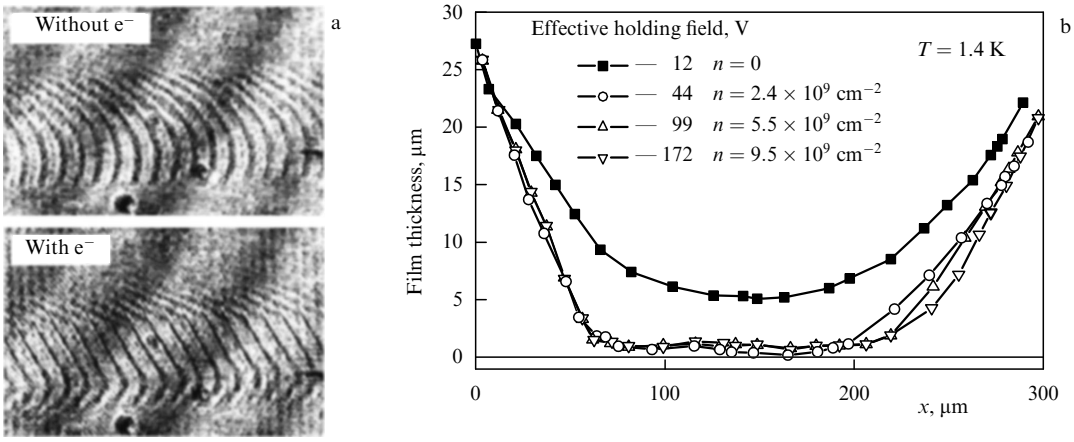


**Figure 25.** Data on the state of a helium film surface in a quasi-one-dimensional cell having the distance between its sides smaller than the capillary constant. In the neutral state, the film forms a well apparent meniscus of finite Laplace radius. Attempts to charge the film and thereby measure the segment of the curve for $n_{\rm cr}(d)$ to the right of its minimum (see Fig. 15) result in deformation of the film shape and stabilization of its geometry at the left shoulder of curve $n_{\rm cr}(d)$ [66].

continuity breaks in the charge density distribution); in this case, there is no regular approach for the scenario with $V = \text{const}$ because of the absence of the perturbation theory in parameter $\kappa\xi_{\max} < 1$ that has here a scale on the order of unity. In these conditions, an equipotential film is an alternative, leaving open the possibility of constructive calculations. Details of this alternative discussed below are qualitatively most interesting for soliton results.

The equation for a small addition $\delta\xi(x)$ to static deformation $\langle\xi\rangle$ within the accuracy of the first nonlinear contribution, namely

$$\xi(x) = \langle\xi\rangle + \delta\xi(x)\,, \qquad \int_{-L}^{+L} \delta\xi(s)\,\mathrm{d}s = 0\,, \tag{3.26}$$

has the form

$$\left[\rho g^* - \frac{V^2}{4\pi(d+\langle\xi\rangle)^3}\right]\delta\xi - \alpha\,\delta\xi'' + \frac{3V^2}{8\pi(d+\langle\xi\rangle)^4}\,\delta\xi^2 = \text{const} = c_0\,. \tag{3.27}$$

The expression in square brackets on the left-hand side of equation (3.27) changes the sign at point

$$4\pi\rho g^*\big(d+\langle\xi\rangle\big)^3 = V_{\rm crit}^2\,. \tag{3.28}$$

Criterion (3.28) corresponds, as in formulas (3.13), (3.14), to the loss of stability of the homogeneous state of a charged helium film.

It is worthwhile to discuss at the level of relations (3.27), (3.28) the difference between the equipotential problems of reconstruction at bulk and film surfaces. To recall, in the former case the question is not the absence of a solution of the reconstruction problem in general, but the impossibility of formulating it in terms of the smallness of parameter $\kappa\delta\xi \ll 1$. In equation (3.27), a different spatial parameter forms: $\tilde\kappa \ll \kappa$ [see formulas (3.27), (3.29), (3.30) containing the definition of this parameter]. Therefore, there is hope of elucidating, even if qualitatively, the structure of a corrugated film surface under conditions of its equipotentiality and the smallness of the parameter $\tilde\kappa\delta\xi \ll 1$ justifying power expansion in this parameter in Eqn (3.27).

In the conditions of $V > V_{\rm crit}$, the first integral of Eqn (3.27) equals

$$\left(\frac{\mathrm{d}\xi(x)}{\mathrm{d}x}\right)^2 = -\frac{\tilde\kappa^2\delta\xi^2}{2} + \frac{\gamma^3\delta\xi^3}{3} + c_0\delta\xi + c_1\,, \tag{3.29}$$

$$\tilde\kappa^2 = \kappa^2\left[\frac{V^2}{4\pi\big(d+\langle\xi\rangle\big)^3\rho g^*} - 1\right], \quad \gamma^3 = \frac{V^2}{4\pi\big(d+\langle\xi\rangle\big)^4\alpha}\,. \tag{3.30}$$

This expression testifies to the formation of a natural region of length $\tilde\kappa^{-1}$ at the center of soliton in which deformation may oscillate.

Let us assume $\delta\xi'|_{x=0} = 0$ for deformation $\delta\xi_0$ at the center of our soliton, and

$$\delta\xi_0 < 0\,. \tag{3.31}$$

This requirement leads to the definition of 'constant' $c_1$ in Eqn (3.29):

$$c_1 = -c_0\delta\xi_0 + \frac{\tilde\kappa^2\delta\xi_0^2}{2} - \frac{\gamma^3\delta\xi_0^3}{3}\,. \tag{3.32}$$

An additional solution [along with the root of Eqn (3.31)] of equation (3.29) exists in the case of independent points with $\mathrm{d}\xi(x)/\mathrm{d}x = 0$, besides the region with $\delta\xi_0$. Here, the lateral film dimension 'enters' the problem. Assuming the parameter $\tilde\kappa \ll \kappa$ to be small but finite, we seek the solution in which external dimensions of the soliton are fixed by conditions $\mathrm{d}\xi(x)/\mathrm{d}x|_{x=\pm L} = 0$ at the boundaries $\pm L \gg \tilde\kappa^{-2} \gg \kappa^{-2}$. Thus, the problem of reconstruction with a single cycle between the cell boundaries is reduced to studying properties of the roots of equation

$$\gamma^3\,\frac{\delta\xi^3 - \delta\xi_0^3}{3} - \tilde\kappa^2\,\frac{\delta\xi^2 - \delta\xi_0^2}{2} + c_0(\delta\xi - \delta\xi_0) = 0\,. \tag{3.33}$$

As mentioned above, this equation has the root $\delta\xi = \delta\xi_0$. Therefore, the cubic equation (3.33) for roots $\delta\xi \neq \delta\xi_0$ simplifies to a quadratic one relating $\delta\xi_L^2$ to $\delta\xi_0$.

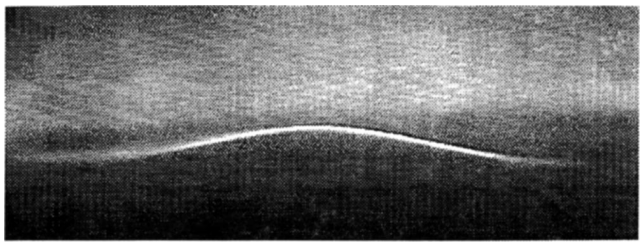

**Figure 26.** Photograph of the charged surface of liquid hydrogen (taken from Ref. [63]). Note the characteristic curvature of the profile (its radius is comparable to the cell's lateral dimensions), much smaller than could be expected from manipulations of the capillary constant alone. The difference is especially well apparent by comparing the soliton tops in this figure and those in Fig. 24.

What follows is just a succinct exposition. The soliton shape is implicitly defined by the second integral of equation (3.27) in the form

$$x = f\left[\delta\xi(x), \delta\xi_0, c_0\right] + c_2\,. \tag{3.34}$$

The new integration constant, $c_2$, follows from the condition $\delta\xi(x \to 0) \to \delta\xi_0$, whence $c_2 = 0$.

The resulting solution must be correlated with the requirement

$$L = f\left[\delta\xi_L(\delta\xi_0), \delta\xi_0, c_0\right]. \tag{3.35}$$

Moreover, there is normalization (3.26). These conditions are sufficient to define the remaining constants $\delta\xi_0$, $c_0$ and thereby to close the discussion of conditions for the existence of a soliton on a bounded equipotential film.

The details being neglected, the resulting solution $\delta\xi(x)$ has the structure

$$\delta\xi(x) \simeq \frac{\tilde{\kappa}^2}{\gamma^3}\left(1 - \tanh^2\frac{\tilde{\kappa}x}{2}\right), \tag{3.36}$$

where $\gamma$ and $\tilde{\kappa}$ are taken from formulas (3.30). A soliton of this type is well known from work on the shallow water theory [67].

Observation of the soliton state on an equipotentially saturated charged hydrogen film in supercritical conditions is reported in paper [63] (Fig. 26). Note a characteristic curvature of the profile, which is much smaller than could be expected from manipulations with the capillary constant alone. For comparison, it is convenient to consider the profile of a multicharged dimple formed by the local pressure of a finite number of charges accumulated on its top (see Fig. 24). The curvature of the central part is controlled here by the capillary constant (as it should be for a cluster with a fixed number of charges in the central part).

Using the definition (3.34), (3.35) of the solution shape, it may be numerically compared with the data of Fig. 26. Relevant treatment yields the result given in Fig. 27.

D. *Concluding the 'soliton' part of this section*. We can afford to go beyond the above framework of reasoning that does not include the domain of essentially nonlinear phenomena at a charged liquid surface. The soliton shown in Fig. 26 that emerged at the flat charged boundary losing its stability in the field $U_{c1}$ of the diagram (see Fig. 24) with an increase in the

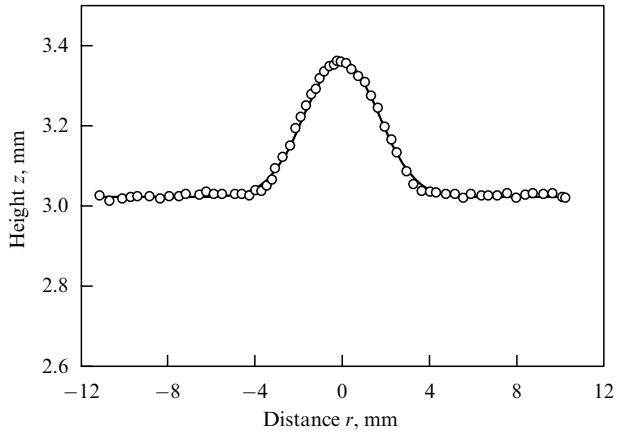


**Figure 27.** Comparison of the soliton shape calculated using formulas (3.34), (3.35) (solid curve) and that shown in Fig. 26 (circles).

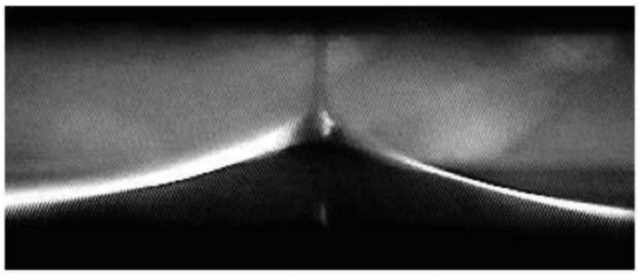

**Figure 28.** The behavior of an equipotential soliton in the vicinity of the upper critical field $U_{c2}$ (data of Fig. 24 from Ref. [63]). In accordance with formulas (3.30), the curvature of the profile at the top of the soliton sharply increases, thus inducing a breakdown and periodic escape of the accumulated charge toward the gate electrode (relaxationally pulsating geyser).

degree of supercriticality up to the $U_{c2}$ level becomes unstable itself and turns into a geyser, periodically breaking through the liquid boundary (Fig. 28); its outburst emits a portion of charges detected by an electrometer (the chronologically first formation of a geyser by positive ions seeking to leave the charged helium surface in a strong electric field was observed in Refs [69, 70] under conditions in which the external receiving electrode was essentially nonplanar).

In this part of the study, the cryogenic problem of developing instability of a charged liquid surface overlaps with research on the properties of normal electrolytes and liquid metals (Fig. 29). The central issue here from both theoretical [69–75] and experimental [71, 72] standpoints is the shape of the surface of a conducting liquid under conditions of developing instability. The construction of theory aims at substantiating the assertion that a soliton in the final phase must, as a rule, have the form of an axisymmetric pyramid with a cone angle of 98.6° (Taylor cone) [71, 72].

There is every reason to believe that cryogenic and normal patterns of an eruption growth for a solitary geyser are identical. The cryogenic conditions allow this process to be observed in the form of reproducible relaxational oscillations [63]. The results of liquid metal research may have practical applications, for example, for the formation and acceleration of bulk charged clusters.

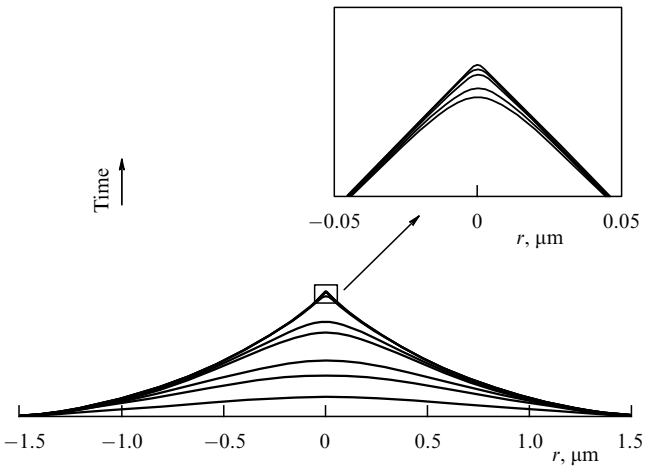


**Figure 29.** The calculated results of the evolving soliton profile for a geyser in a metal [69, 70]. The arrow indicates the direction of time evolution of the soliton shape. There is an obvious analogy with data presented in Fig. 28.

## 4. Conclusions

In conclusion, the present review concerning the problem posed in Ref. [16] systematizes the currently available information on stability and reconstruction of flat charged surfaces of cryogenic liquids under conditions different in terms of cell geometry, external electrostatics, degree of electron filling, etc. Prospects for the further development of research on this topic are outlined.

It was shown that reconstruction of a charged liquid surface proceeds under different scenarios, depending on a combination of external conditions.

(1) In neutral liquid dielectrics (magnetic materials), the boundary stability is disturbed at a finite wave number $q \simeq a^{-1}$ of the dispersion law $\omega(q)$ for small oscillations of the shape of the free liquid surface in an external electric field (here, $a$ is the so-called capillary length). Reconstruction of the free liquid surface (i.e., its transition from the flat to the corrugated state) is possible and realized in the so-called homogeneous scenario where the electrostatic boundary conditions along the corrugated liquid surface are homogeneous over its entire profile. The systematic description of corrugation is feasible only in the presence of the small parameter $(\epsilon_1 - \epsilon_2)/(\epsilon_1 + \epsilon_2) \ll 1$. The period of developing corrugation is scaled by the capillary length. Observations confirm the existence of such reconstruction (see review [16]) and the requirements for the smallness of the parameter are not very stringent, playing a special role only in theoretical considerations.

(2) The establishment of finite charge density at the liquid–vapor interface at a fixed total charge number results in a wide diversification of reconstruction details. An additional parameter $v$, the degree of filling this interphase boundary with charges (with respect to the critical one), appears in the problem: $0 < v \leqslant 1$. On the whole, the reconstruction is inhomogeneous because the entire interface breaks into a system of multicharged dimples. At different poles of filling $v$, corrugation varies from periodic (with a period on the order of capillary length and signs of similarity with spinodal decay processes) in the region of $v \leqslant 1$ to the state characterized by the appearance of individual binodal solitons with a charged nucleus and neutral wings, as $v \to 0$. Transition in the vicinity of $v \leqslant 1$ has much in common with spinodal decay in the physics of first-order phase transitions.

Experimental studies of the inhomogeneous reconstruction of charged cryogenic liquid surfaces are far ahead of research on other possible scenarios of this beautiful effect and confirm many details ensuing from the theory of this phenomenon.

It is possible to create conditions for the homogeneous development of events on a maximally charged liquid surface (liquid metal in an electric field). In this case, however, the theory does not contain small parameters and therefore remains undeveloped. Being focused on the observation of different types of geysers, experiments with liquid metals have not thus far revealed a finite reconstruction.

(3) Thin charged liquid films lose stability at small (formally, zero) wave numbers. This fact is of significance for reconstruction phenomena, accounting for an alternative-to-dispersion scenario of developing instability of a flat charged liquid film. The role of van der Waals forces is of special importance and interest for the development of charged film stability criteria. The reconstruction takes place, but differs from that in the 'bulk' problem. The notion of an individual multicharged dimple is modified, too. Reconstruction of a charged liquid film with metallic properties becomes possible (in contrast to the 'bulk' problem).

There are experimental constraints on the creation of film systems with large lateral dimensions. As a result, the observed reconstruction has the form of individual visible solitons with predictably varying properties.

**Acknowledgments**

The author gratefully acknowledges L P Pitaevskii for discussions of the problem in general and valuable comments. I would like to thank P Leiderer, F I B Williams, M S Khaikin, L P Mezhov-Deglin, A A Levchenko, S S Nazin, V S Edel'man, and G V Kolmakov for the long-term fruitful collaboration, joint work, and numerous discussions. I am also thankful to E V Lebedeva and E A Klinova for taking interest in the problem and their participation in calculations and graphic design of the results. The work was partly supported by RFBR grant No. 09-02-00894 and the Program 'Physics of Condensed Media' of the Presidium of the Russian Academy of Sciences.

## References

1. Frenkel Ya *Zh. Eksp. Teor. Fiz.* **9** 641 (1939)
2. Landau L D, Lifshitz E M *Elektrodinamika Sploshnykh Sred* (Electrodynamics of Continuous Media) (Moscow: Fizmatgiz, 1959) [Translated into English (Oxford: Pergamon Press, 1960)]
3. Bohr N, Wheeler J A *Phys. Rev.* **56** 426 (1939)
4. Frenkel J *Phys. Z. Sowjetunion* **8** 675 (1935)
5. Frenkel Ya *Zh. Eksp. Teor. Fiz.* **6** 347 (1936)
6. Tonks L *Phys. Rev.* **48** 562 (1935)
7. Melcher J R *Field-coupled Surface Waves* (Cambridge, Mass.: M.I.T. Press, 1963)
8. Taylor G I, McEwan A D *J. Fluid Mech.* **22** 1 (1965)
9. Cowley M D, Rosensweig R E *J. Fluid Mech.* **30** 671 (1967)
10. Strutt J W (Baron Rayleigh) *The Theory of Sound* Vol. 2 (London: Macmillan, 1878) [Translated into Russian (Moscow: Gostekhizdat, 1955)]
11. Batchelor G K *An Introduction to Fluid Dynamics* (Cambridge: Univ. Press, 1967) [Translated into Russian (Moscow: Mir, 1973)]
12. Landau L D, Lifshitz E M *Gidrodinamika* (Fluid Mechanics) (Moscow: Nauka, 1988) [Translated into English (Oxford: Pergamon Press, 1987)]

13. Behringer R P *Rev. Mod. Phys.* **57** 657 (1985)
14. Zaitsev V M, Shliomis M I *Dokl. Akad. Nauk SSSR* **188** 1261 (1969) [*Sov. Phys. Dokl.* **14** 1001 (1970)]
15. Gailitis A *Magn. Gidrodin.* **5** (1) 68 (1969) [*Magnetohydrodynamics* **5** (1) 44 (1969)]
16. Shliomis M I *Usp. Fiz. Nauk* **112** 427 (1974) [*Sov. Phys. Usp.* **17** 153 (1974)]
17. Chernikova D M *Zh. Eksp. Teor. Fiz.* **68** 249 (1975) [*Sov. Phys. JETP* **41** 121 (1975)]
18. Gor'kov L P, Chernikova D M *Dokl. Akad. Nauk SSSR* **228** 829 (1976) [*Sov. Phys. Dokl.* **21** 328 (1976)]
19. Kuznetsov E A, Spektor M D *Zh. Eksp. Teor. Fiz.* **71** 262 (1976) [*Sov. Phys. JETP* **44** 136 (1976)]
20. Ikezi H *Phys. Rev. Lett.* **42** 1688 (1979)
21. Leiderer P, Wanner M *Phys. Lett. A* **73** 189 (1979)
22. Ebner W, Leiderer P *Phys. Lett. A* **80** 277 (1980)
23. Mel'nikov V I, Meshkov S V *Pis'ma Zh. Eksp. Teor. Fiz.* **33** 222 (1981) [*JETP Lett.* **33** 211 (1981)]
24. Mel'nikov V I, Meshkov S V *Zh. Eksp. Teor. Fiz.* **81** 951 (1981) [*Sov. Phys. JETP* **54** 505 (1981)]
25. Mel'nikov V I, Meshkov S V *Zh. Eksp. Teor. Fiz.* **82** 1910 (1982) [*Sov. Phys. JETP* **55** 1099 (1982)]
26. Gianetta R W, Ikezi H *Phys. Rev. Lett.* **47** 849 (1981)
27. Gianetta R W, Ikezi H *Surf. Sci.* **113** 412 (1982)
28. Leiderer P, Ebner W, Shikin V B *Surf. Sci.* **113** 405 (1982)
29. Malyarov V V *Osnovy Teorii Atomnogo Yadra* (Fundamentals of the Atomic Nucleus Theory) (Moscow: Nauka, 1967)
30. Shikin V B *Pis'ma Zh. Eksp. Teor. Fiz.* **27** 44 (1978) [*JETP Lett.* **27** 39 (1978)]
31. Salomaa M M, Williams G A *Phys. Rev. Lett.* **47** 1730 (1981)
32. Nazin S S, Izotov A N, Shikin V B *Dokl. Akad. Nauk SSSR* **283** 121 (1985) [*Sov. Phys. Dokl.* **20** 606 (1985)]
33. Albrecht U, Leiderer P *Europhys. Lett.* **3** 705 (1987)
34. Dalfovo F et al. *Rev. Mod. Phys.* **71** 463 (1999)
35. Nauta K, Miller R E *J. Chem. Phys.* **115** 10254 (2001)
36. Makarov G N *Usp. Fiz. Nauk* **174** 225 (2004) [*Phys. Usp.* **47** 217 (2004)]
37. Zharov A N, Shiryaeva S O, Grigor'ev A I *Zh. Tekh. Fiz.* **74** (7) 19 (2004) [*Tech. Phys.* **49** 824 (2004)]
38. Crandall R S *Surf. Sci.* **58** 266 (1976)
39. Gor'kov L P, Chernikova D M *Pis'ma Zh. Eksp. Teor. Fiz.* **18** 119 (1973) [*JETP Lett.* **18** 68 (1973)]
40. Volodin A P, Khaikin M S, Édel'man V S *Pis'ma Zh. Eksp. Teor. Fiz.* **26** 707 (1977) [*JETP Lett.* **26** 543 (1977)]
41. Leiderer P *Phys. Rev. B* **20** 4511 (1979)
42. Shikin V *Pis'ma Zh. Eksp. Teor. Fiz.* **78** 930 (2003) [*JETP Lett.* **78** 461 (2003)]
43. Chernikova D M *Zh. Eksp. Teor. Fiz.* **68** 249 (1975) [*Sov. Phys. JETP* **41** 121 (1975)]
44. Shikin V B, Leiderer P *Pis'ma Zh. Eksp. Teor. Fiz.* **32** 439 (1980) [*JETP Lett.* **32** 416 (1980)]
45. Shikin V B, Leiderer P *Zh. Eksp. Teor. Fiz.* **81** 184 (1981) [*Sov. Phys. JETP* **54** 92 (1981)]
46. Landau L D *Zh. Eksp. Teor. Fiz.* **7** 19 (1937); *Phys. Z. Sowjetunion* **11** 26 (1937)
47. Olemskoi A I, Koplyk I V *Usp. Fiz. Nauk* **165** 1105 (1995) [*Phys. Usp.* **38** 1061 (1995)]
48. Morse P M, Feshbach H *Methods of Theoretical Physics* Vol. 2 (New York: McGraw-Hill, 1953) [Translated into Russian (Moscow: IL, 1960)]
49. Leiderer P, Shikin V *J. Low Temp. Phys.* **162** 693 (2011)
50. Shikin V B *Zh. Eksp. Teor. Fiz.* **86** 521 (1984) [*Sov. Phys. JETP* **59** 304 (1984)]
51. Bonsall L, Maradudin A A *Phys. Rev. B* **15** 1959 (1977)
52. Ikezi H, Giannetta R W, Platzman P M *Phys. Rev. B* **25** 4488 (1982)
53. Chernikova D M *Fiz. Nizk. Temp.* **2** 1374 (1976) [*Sov. J. Low Temp. Phys.* **2** 669 (1976)]
54. Peeters F M *Phys. Rev. B* **30** 159 (1984)
55. Sabisky E S, Anderson C H *Phys. Rev. A* **7** 790 (1973)
56. Putterman S J *Superfluid Hydrodynamics* (Amsterdam: North-Holland Publ. Co., 1974)
57. Etz H et al. *Phys. Rev. Lett.* **53** 2567 (1984)
58. Tatarskii V V *Fiz. Nizk. Temp.* **12** 451 (1986) [*Sov. J. Low Temp. Phys.* **12** 255 (1986)]
59. Tatarskii V V *Fiz. Nizk. Temp.* **10** 435 (1984) [*Sov. J. Low Temp. Phys.* **10** 227 (1984)]
60. Valdesh A, Diplom (Gif-sur-Yvette: Centre CEA de Saclay, 1980)
61. Shikin V, Leiderer P *Fiz. Nizk. Temp.* **23** 624 (1997) [*Low Temp. Phys.* **23** 468 (1997)]
62. Shikin V B, Lebedeva E V *Fiz. Nizk. Temp.* **24** 299 (1998) [*Low Temp. Phys.* **24** 225 (1998)]
63. Levchenko A A et al. *Fiz. Nizk. Temp.* **25** 333 (1998) [*Low Temp. Phys.* **25** 242 (1999)]
64. Günzler T, Ph.D. Thesis (Konstanz: Konstanz Univ., 1994)
65. Shikin V B, Lebedeva E V *Pis'ma Zh. Eksp. Teor. Fiz.* **57** 126 (1993) [*JETP Lett.* **57** 135 (1993)]
66. Valkering A, Klier J, Leiderer P *Physica B* **284 – 288** 172 (2000)
67. Lavrent'ev M A, Shabat B V *Metody Teorii Funktsii Kompleksnogo Peremennogo* (Methods of the Theory of Complex Variable Functions) (Moscow: Fizmatgiz, 1958)
68. Volodin A P, Khaikin M S *Pis'ma Zh. Eksp. Teor. Fiz.* **30** 608 (1979) [*JETP Lett.* **30** 572 (1979)]
69. Suvorov V G *Pis'ma Zh. Tekh. Fiz.* **26** (1) 66 (2000) [*Tech. Phys. Lett.* **26** 33 (2000)]
70. Suvorov V G, Thesis for Cand. Phys.-Math. Sci. (Ekaterinburg: IEP UB RAS, 2001)
71. Taylor G *Proc. R. Soc. London A* **280** 383 (1964)
72. Gabovich M D, Poritskii V Ya *Pis'ma Zh. Eksp. Teor. Fiz.* **33** 320 (1981) [*JETP Lett.* **33** 304 (1981)]
73. Zubarev N M *Pis'ma Zh. Eksp. Teor. Fiz.* **73** 613 (2001) [*JETP Lett.* **73** 544 (2001)]
74. Zubarev N M *Zh. Eksp. Teor. Fiz.* **121** 624 (2002) [*JETP* **94** 534 (2002)]
75. Zubarev N M, Thesis for Doct. Phys.-Math. Sci. (Ekaterinburg: IEP UB RAS, 2002)